© 2019. Published by The Company of Biologists Ltd | Disease Models & Mechanisms (2019) 12, dmm039636. doi:10.1242/dmm.039636

REVIEW

Photoacoustic imaging as a tool to probe the tumour microenvironment

Emma Brown[1,2], Joanna Brunker[1,2] and Sarah E. Bohndiek[1,2,*]

ABSTRACT

The tumour microenvironment (TME) is a complex cellular ecosystem subjected to chemical and physical signals that play a role in shaping tumour heterogeneity, invasion and metastasis. Studying the roles of the TME in cancer progression would strongly benefit from non-invasive visualisation of the tumour as a whole organ *in vivo*, both preclinically in mouse models of the disease, as well as in patient tumours. Although imaging techniques exist that can probe different facets of the TME, they face several limitations, including limited spatial resolution, extended scan times and poor specificity from confounding signals. Photoacoustic imaging (PAI) is an emerging modality, currently in clinical trials, that has the potential to overcome these limitations. Here, we review the biological properties of the TME and potential of existing imaging methods that have been developed to analyse these properties non-invasively. We then introduce PAI and explore the preclinical and clinical evidence that support its use in probing multiple features of the TME simultaneously, including blood vessel architecture, blood oxygenation, acidity, extracellular matrix deposition, lipid concentration and immune cell infiltration. Finally, we highlight the future prospects and outstanding challenges in the application of PAI as a tool in cancer research and as part of a clinical oncologist's arsenal.

KEY WORDS: Optoacoustic imaging, Hypoxia, Cancer, TME, PAI, Vasculature

Introduction

The focus of cancer research has moved from treating the tumour as a homogenous mass of cancer cells to considering the wider tumour microenvironment (TME; see Box 1 for a glossary of terms) (Quail and Joyce, 2013). The infrastructure of a growing solid tumour is a heterogeneous mixture of cancer and stromal cells. In addition to this complex cellular picture, chemical signals such as hypoxia (Box 1) and physical signals arising from fibrosis (Box 1), among others (Fig. 1), are linked to poor patient prognosis (Gilkes et al., 2014). Importantly, these features of the TME interact with and regulate one another (De Palma et al., 2017; Kalluri, 2016; LaGory and Giaccia, 2016), and such dynamic relationships influence tumour growth and heterogeneity.

Improving our understanding of the role of the TME in cancer progression would strongly benefit from non-invasive visualisation of the tumour as a whole organ *in vivo*, both preclinically in mouse models of the disease, as well as in patients. Unfortunately, features of the TME remain challenging to resolve with non-invasive imaging. As a result, many studies still rely on excised tissues *ex vivo*, which only interrogate a small portion of the tumour at a fixed time point, and are not able to capture its full spatial and temporal heterogeneity. Visualising the dynamic TME *in vivo* would allow researchers to investigate key questions about the interplay between different features of the microenvironment, for example, the functional relationship between hypoxia and fibrosis (Gilkes et al., 2014). The biomarkers resulting from these studies could then be applied clinically to predict tumour aggressiveness, stratify patients and monitor treatment response. Ultimately, this would transform patient care and improve survival by helping to guide therapeutic strategies (Abadjian et al., 2017; Weissleder et al., 2016).

A range of existing *in vivo* imaging techniques can be used to visualise different facets of the TME and have already provided valuable insight. Unfortunately, they come with limitations that include limited spatial resolution, extended scan times and poor specificity from confounding signals. Photoacoustic (also referred to as optoacoustic) imaging (PAI; Box 1) is a promising technique with potential to overcome these limitations for imaging TME features *in vivo*. This Review will first introduce key aspects of the TME, focusing on tumour vasculature and hypoxia, the extracellular matrix (ECM; Box 1) and lipids, together with the immune cell compartment, explaining their individual importance in cancer biology and their dynamic interactions as a microenvironment. We will then review the advantages and disadvantages of current techniques for imaging these key components *in vivo* and specifically focus on the potential of PAI in such studies. We conclude by discussing the potential of PAI for clinical imaging of the TME and the outstanding challenges that must be overcome to achieve this.

Features of the TME

Tumour vasculature and hypoxia in the TME

A growing tumour mass requires a vascular network to supply cancer cells with nutrients and remove metabolic waste products, which then permits cancer cells to extravasate and metastasise. Development of a vascular network typically begins in response to diffusion-limited or chronic hypoxia, which arises when the diffusion of oxygen from surrounding blood vessels is insufficient to meet the demand of the proliferating cancer cells (LaGory and Giaccia, 2016; Lundgren et al., 2007). Activation of hypoxia-inducible factors (HIFs) drives the transcription of genes involved in a wide range of cellular functions (LaGory and Giaccia, 2016; Lundgren et al., 2007), including the production of pro-angiogenic factors, such as vascular endothelial growth factor (VEGF), that stimulate endothelial cells to proliferate, sprout and form new blood vessels (Folkman, 1971; Hoeben et al., 2004). Often an imbalance of pro- and anti-angiogenic factors then occurs, which results in a chaotic and heterogeneous network of blood vessels, including

[1]Department of Physics, University of Cambridge, JJ Thomson Avenue, Cambridge CB3 0HE, UK. [2]Cancer Research UK Cambridge Institute, University of Cambridge, Li Ka Shing Centre, Robinson Way, Cambridge CB2 0RE, UK.

*Author for correspondence (seb53@cam.ac.uk)

S.E.B., 0000-0003-0371-8635

Disease Models & Mechanisms (2019) 12, dmm039636. doi:10.1242/dmm.039636

Box 1. Glossary

Absorption coefficient: the fraction of incident radiant energy absorbed per unit mass or thickness of an absorber.
Angiogenesis: the development of new blood vessels from pre-existing vessels. Driven by pro-angiogenic factors such as VEGF and inhibited by anti-angiogenic factors.
Contrast agent: a substance or molecule that is administered into a living subject to enhance the visualisation of a particular structure or biological process within the body in medical imaging.
Extracellular matrix (ECM): a three-dimensional, non-cellular structure produced and secreted by cells. It is composed primarily of fibrous elements such as collagen and forms the interstitial connective tissue and the basement membrane.
Fibrosis: the thickening and scarring of connective tissue, usually as a result of injury.
Hypoxia: a deficiency in the amount of oxygen reaching tissues.
Isosbestic point: a wavelength at which the absorption coefficient of two molecules is equal.
Light fluence: optical energy per unit area.
Optical diffusion limit: the depth in biological tissue beyond which light propagating along the predefined linear trajectory becomes too weak to be detected in practice (Wang and Hu, 2012).
Perfusion: the flow rate of blood per mass of tissue.
Photoacoustic (optoacoustic) imaging (PAI): a biomedical imaging modality based on the photoacoustic effect.
Photoacoustic effect: the generation of sound waves following light absorption in a material such as tissue.
Tumour microenvironment (TME): the cellular environment in which a tumour exists, including blood vessels, fibroblasts, immune cells and the ECM.

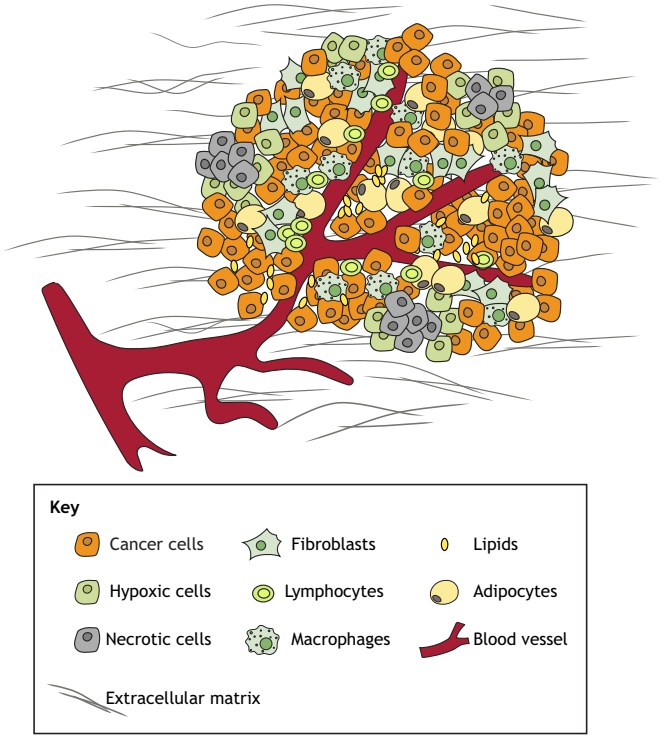

Fig. 1. The tumour microenvironment (TME). Schematic diagram illustrating the involvement of multiple cell types in a tumour, including endothelial cells and pericytes that make up blood vessels, as well as immune cells, fibroblasts and adipocytes, alongside the cancer cells. Lipids are synthesised by adipocytes and cancer cells. Hypoxia arises as the tumour grows beyond the limit of oxygen diffusion from the surrounding vessels. Fibrosis arises from excessive deposition of extracellular matrix (ECM) components without concurrent degradation. A supportive environmental niche of these chemical and physical signals evolves with the cancer cells to promote tumour development and progression.

many immature vessels with poor pericyte coverage (Ribeiro and Okamoto, 2015), irregular branching and a tortuous morphology (Hanahan and Weinberg, 2011; Krishna Priya et al., 2016; Nagy and Dvorak, 2012; Nagy et al., 2007).

Several important prognostic consequences arise from these features of the tumour vasculature. Firstly, perfusion-limited (Box 1), or cycling, hypoxia occurs in cancer and stromal cells adjacent to the immature tumour blood vessels, generating repeated dynamic cycles of ischaemia and reperfusion that produce oxidative stress, which leads to increased stem-cell-like properties of cancer cells and resistance to therapy (Michiels et al., 2016). Secondly, heterogeneity of vessel perfusion leads to unequal access of systemic therapeutic agents within the tumour. Although some areas of the tumour – those that are well perfused – will likely receive the expected therapeutic dose, other poorly perfused areas may receive a lower dose, meaning that they can survive the treatment (Trédan et al., 2007). Finally, as tumours shift to a predominantly glycolytic metabolism via the expression of HIF target genes, poor perfusion allows lactic acid (from anaerobic glycolysis) and protons (from the conversion of CO_2 produced from the pentose phosphate pathway) to accumulate in the TME, giving rise to acidosis (Parks and Pouysségur, 2017; Parks et al., 2010). Acidosis can increase cancer cell invasion (Estrella et al., 2013) and metastatic potential (Rofstad et al., 2006), and decrease drug efficacy (Vukovic and Tannock, 1997). The HIF1α, VEGF and associated pathways are linked to poor prognosis in a range of solid tumours (Hegde et al., 2013; Lundgren et al., 2007; Semenza, 2016), demonstrating the consequences of tumour hypoxia on patient outcome.

ECM and lipid composition of the TME

The tissue ECM is a three-dimensional, non-cellular structure composed primarily of collagen, which forms the interstitial connective tissue and the basement membrane. ECM function extends beyond physical support to directly influence cell growth and motility. Dysregulation of ECM remodelling in cancer leads to excessive production and deposition of ECM proteins, termed fibrosis (Lu et al., 2012), which drives tumour progression by: stimulating cancer cell proliferation (Levental et al., 2009); changing cancer cell contractility, polarity and mechanosignalling (Gilkes et al., 2014); providing a reservoir of growth factors and pro-angiogenic factors (Bonnans et al., 2014; De Palma et al., 2017); and promoting epithelial-to-mesenchymal transition (EMT) (Zhang et al., 2013). It is therefore unsurprising that increased expression of ECM remodelling genes, particularly in breast cancer, leads to higher mortality (Chang et al., 2005). Although the absence of fibrotic foci does not necessarily indicate benignity, highly fibrotic breast tumours have a poor prognosis (Conklin et al., 2011), with a high risk of recurrence (Hasebe et al., 1997).

The lipid content of tumours is significantly different from that of healthy tissues and plays an important role in the TME, particularly in lipid-rich tissues such as the breast (Baenke et al., 2013; Choi et al., 2018). Fatty acids, arising from adipocytes or synthesised by cancer cells themselves in *de novo* lipogenesis, can provide cancer cells with an alternative energy source in times of chronic nutrient depletion, which may be spatially heterogeneous and relates to the state of tumour perfusion (Baenke et al., 2013; Choi et al., 2018; Kuhajda et al., 1994; Michiels et al., 2016; Walter et al., 2009). In addition to providing an alternative energy source, lipids have

Disease Models & Mechanisms (2019) 12, dmm039636. doi:10.1242/dmm.039636

structural roles in phospholipid membranes, which are needed for cell proliferation, and lipid mediators such as prostaglandin E2 promote cancer cell proliferation and survival via MAPK signalling (Krysan et al., 2005).

Cellular components of the TME

The presence of endothelial cells, adipocytes and fibroblasts in the TME serve to define the aforementioned environmental features. Cancer-associated fibroblasts (CAFs) are the predominant stromal cell type secreting ECM in the TME and have a complex role that has been extensively reviewed elsewhere (Kalluri, 2016; LeBleu and Kalluri, 2018). It is worth noting that, in addition to ECM production, CAFs secrete matrix metalloproteases (MMPs) (reviewed in LeBleu and Kalluri, 2018). MMPs break down ECM and basement membrane, promoting cancer cell invasion and EMT. Endothelial cells also secrete MMPs to allow sprouting and angiogenesis (Box 1) (reviewed in Egeblad and Werb, 2002; Kalluri, 2016).

However, a major cellular component that merits discussion is the immune cell infiltrate. It is now well known that immune cells play a vital role in tumour development (Fridman et al., 2017; Joyce and Fearon, 2015), which has led to the recent emergence of immunotherapy strategies (reviewed in Rosenberg and Restifo, 2015; Sharma and Allison, 2015). The dual role of immune cells in the TME is exemplified by the fact that cancer cells evade the immune system in order to survive (Sharma and Allison, 2015), while, on the other hand, many immune cell types release immunosuppressive cytokines and act in a pro-tumorigenic manner (Box 2).

Monitoring tumour response to immunotherapy is currently a major clinical challenge due to the dynamic nature of the immune TME. To optimise immunotherapy use whilst minimising toxicity and cost in non-responders, appropriately validated non-invasive imaging techniques could be applied to monitor the evolution of the TME in response to immunotherapy in real time and avoid repeated tissue sampling (Gibson et al., 2018; Mehnert et al., 2017; Schuurhuis et al., 2009; Tavaré et al., 2014). There is currently no single accurate biomarker to stratify patients for immunotherapy; it is likely that multiple biomarkers will need to be used together to give an accurate representation of a patient's TME (Gibney et al., 2016; Mehnert et al., 2017).

Dynamic interactions of TME features

It is increasingly evident that features of the TME regulate each other. Hypoxia plays a central role in these interactions. For example, increased deposition of ECM proteins and recruitment of stromal cells leads to fibrotic contraction of the interstitial tissue space, which is associated with: increased interstitial fluid pressure (Heldin et al., 2004); the collapse of immature blood vessels; and restricted oxygen diffusion, which causes hypoxia (Jain et al., 2014). Conversely, at the molecular level, HIF1α directly activates transcription of genes required for collagen synthesis and cross-linking, such as procollagen lysyl hydroxylase 2 (Erler et al., 2006; Gilkes et al., 2013a,b), which increases angiogenic signalling and vessel permeability (Bordeleau et al., 2017; Saupe et al., 2013). This could actually result in decreased oxygen delivery to the tumour and thus further hypoxia.

The pro-angiogenic signalling of many stromal cell types is also hypoxia-mediated. Hypoxia drives macrophage polarisation towards an M2 phenotype (Box 2), which is anti-inflammatory and pro-angiogenic (Colegio et al., 2014). Many M2 macrophages are $Tie2^{+}$ and cluster around existing blood vessels, promoting angiogenesis (Britto et al., 2018; De Palma et al., 2003, 2005; Hughes et al., 2015) and vessel permeability (Stockmann et al., 2008). The milieu of cytokines and growth factors secreted by CAFs contain further pro-angiogenic factors (De Palma et al., 2017), while hypoxia upregulates the production of sphingosine lipids (Ahmad et al., 2006; Pyne and Pyne, 2010) that are also likely to drive angiogenesis (Baenke et al., 2013; Nakajima et al., 2017). Additionally, hypoxia and acidosis modulate the function of all immune cell types, meaning that hypoxic niches spatially fine-tune the TME (Calcinotto et al., 2012; LaGory and Giaccia, 2016).

Finally, many therapies modulate the evolution of the TME and the dynamic relationships within. Anti-angiogenic treatments, which often target the VEGF pathway, have been shown to 'normalise' tumour vasculature by increasing vessel maturity, leading to re-oxygenation of the tumour and decreased hypoxia in mouse models (Dickson et al., 2007; Winkler et al., 2004). As mentioned above, immunotherapies such as checkpoint receptor inhibitors (Box 2) aim to overcome the negative regulation of immune cells in the TME (Joyce and Fearon, 2015) and have been particularly successful in melanoma patients displaying a large immune infiltrate (Hodi et al., 2010).

Box 2. The immune system in the tumour microenvironment

Anti-tumour immunity

Immune cells can recognise cancer cells as foreign and initiate an immune response against them (see the following reviews for more detail: Blomberg et al., 2018; Joyce and Fearon, 2015). This is normally initiated in the same way the immune system recognises and kills foreign pathogens. A tumour-specific antigen released by cancer cells is taken up by dendritic cells (DCs), which are part of the innate immune system. Under pro-inflammatory signals from the tumour microenvironment (TME), DCs migrate to the nearest lymph node, where they interact with and activate T cells, which are part of the adaptive immune system. CD8+ cytotoxic T cells specific to the tumour antigen migrate from the lymph node back to the tumour to kill cancer cells that express the antigen. Ideally, the adaptive immune response should generate immunological memory, meaning that the CD8+ T cells will expand and kill any future cancer cells expressing the same tumour-specific antigen. This is in contrast to innate immune cells, which generally recognise foreign antigens and activate the adaptive immune system. Innate immune cells such as natural killer cells can also kill cancer cells. Unfortunately, cancer cells develop many mechanisms to evade anti-tumour immunity and survive, for example by expressing immune checkpoint receptors. When these receptors bind to CD8+ T cells, they cause the T cell to become deactivated (anergic) and unable to carry out its cytotoxic functions. Immunotherapies such as checkpoint receptor inhibitors aim to increase anti-tumour immunity by blocking these immunosuppressive signals (Sharma and Allison, 2015).

Pro-tumour immunity

Cancer cells can also evade the anti-tumour immune response via pro-tumour immune cells. Cytokines such as TGF-β and IL-10 released by cancer cells or other stromal cells such as cancer-associated fibroblasts (CAFs) can skew CD4+ T-helper cells to become immunosuppressive and begin to inhibit the effect of cytotoxic cell types. Innate immunosuppressive cells such as tumour-associated macrophages (TAMs) are also anti-inflammatory and pro-angiogenic, driving tumour progression (Blomberg et al., 2018). TAMs are often considered to have a classical 'M2' anti-inflammatory phenotype, although there are some differences in gene expression (Franklin et al., 2014). This is in contrast to the pro-inflammatory 'M1' phenotype; however, the subsets of macrophages in the TME should be considered as more of a spectrum of phenotypes, rather than two distinct groups (Hobson-Gutierrez and Carmona-Fontaine, 2018).

These dynamic relationships paint a complicated picture of the TME that will be explored for many years to come. Being able to monitor the dynamics of the TME *in vivo* is therefore essential to improve our understanding of tumour biology and ultimately improve treatments for patients.

Visualising the TME

Existing imaging modalities

Several preclinical and clinical imaging techniques are already available to probe various features of the TME (Table 1). Vascular perfusion can be visualised using intravenous administration of a contrast agent through 'dynamic contrast-enhanced' approaches (Box 1) (Alonzi et al., 2007; Ohno et al., 2014; Saini and Hoyt, 2014), which, despite being widely used, do have some associated toxicity concerns (Heiken, 2008; Rogosnitzky and Branch, 2016).

Hypoxia represents a challenge for imaging in medical diagnostics, as the method must generate a positive signal for the absence of oxygen. Preclinical studies using intravital imaging have revealed blood flow fluctuations and perivascular changes in hypoxia (Michiels et al., 2016), but these approaches have limited prospect for routine clinical use because they are invasive (Table 1). Magnetic resonance imaging (MRI)-based approaches such as blood-oxygen-level-dependent (BOLD) MRI (Hoskin et al., 2007) and oxygen-enhanced (OE) MRI (O'Connor et al., 2016) correlate with tissue oxygenation and histological markers of hypoxia (Hoskin et al., 2007; O'Connor et al., 2016). However, they suffer from intrinsically low sensitivity (Hallac et al., 2014; Howe et al., 2001). Positron emission tomography (PET) agents for hypoxia visualisation, including those derived from nitroimidazole, are also available (Koch and Evans, 2015; Lopci et al., 2014), but application to studying the TME is limited by the inherently low spatial resolution of PET and the requirement to administer a radiopharmaceutical. Diffuse optical spectroscopic imaging (DOSI) is a low-cost and readily accessible approach that measures local optical absorption coefficient (Box 1). DOSI can measure concentrations of oxy- and deoxy-haemoglobin (HbO_2 and Hb, respectively) as surrogate markers of hypoxia (Cerussi et al., 2006; Di Leo et al., 2017; Tromberg et al., 2005) but has poor resolution at depths beyond ∼1 mm due to light scattering in tissue (see 'optical diffusion limit' in Box 1) (Wang and Hu, 2012).

A number of modalities can image fibrosis and lipids (Table 1). Dynamic contrast-enhanced (DCE)–computed-tomography (CT) is clinically approved for imaging tumour fibrosis but it measures interstitial tissue volume, so can be confounded by oedema and necrosis (Koyasu et al., 2016). Diffusion-weighted (DW) MRI, as well as ultrasound and MR-based elastography methods, can image fibrosis but are non-specific and generally have low sensitivity (Muzard et al., 2009; Talwalkar et al., 2007; Taouli et al., 2007). Ultrasound elastography can also have technical failures if obesity or ascites are present, although using MRI elastography instead may overcome this problem (Akkaya et al., 2018). Lipids can be detected in tumours by using MRI (Pokharel et al., 2013), and imaging the rate of fatty acid synthesis is possible with PET agents (Lewis et al., 2014; Schöder and Larson, 2004), but, due to the disadvantages described above, PET is not used regularly.

Preclinical tracking of CAFs, the predominant ECM-producing cell type (Kalluri, 2016), has been achieved using a PET tracer to target fibroblast activation protein (FAP) expressed on CAFs (Giesel et al., 2019), and intravital microscopy in transgenic mice with fibroblasts expressing a green fluorescent reporter protein (Arina et al., 2016). Tracking cells *in vivo* with reporter gene technology is ideal, as daughter cells will also express the reporter, meaning the contrast agent is not diluted. However, as it requires genetic manipulation, reporter gene technology has not yet been translated into clinical applications (Ramamonjisoa and Ackerstaff, 2017).

Despite overwhelming evidence for the importance of immune cells in tumour biology (Fridman et al., 2017; Joyce and Fearon, 2015), there is currently no clinical *in vivo* imaging method approved to visualise immune cells in the TME. Intravital microscopy and PET are most commonly employed in the research setting (Table 1). Intravital imaging of immune cells expressing a fluorescent reporter gene provides single-cell resolution and has revealed new immune-cell–tumour-cell interactions in preclinical models (Hanna et al., 2015, 2016). ^{18}F-fluorodeoxyglucose PET is used to monitor tumour glucose metabolism and could also monitor inflammatory cell infiltration, as these cells are also glycolytic (Hammoud, 2016; Kostakoglu et al., 2003; Wu et al., 2013). Researchers also developed PET agents to specifically track immune cell populations and cytokines and monitor response to immunotherapy (Gibson et al., 2018; Larimer et al., 2016, 2017; Maute et al., 2015; Natarajan et al., 2017; Tavaré et al., 2014). Radiolabelled antibodies have been used to label T-cell populations (Larimer et al., 2016; Natarajan et al., 2017; Tavaré et al., 2014) as these cells infiltrate the tumour and can predict immunotherapy response (Larimer et al., 2016). In the clinic, anatomical CT images of patients on immunotherapy have shown a 'pseudoprogression' effect, whereby tumour size initially increases due to abundant T-cell infiltrate and, later, tumour size decreases in responders (Nishino et al., 2018).

Notably, many of the techniques described here suffer from limited spatial resolution, poor specificity from confounding signals and the need to administer contrast agents (Table 1). Additionally, none of the techniques described reveal multiple features of the TME within the same imaging scan. Mapping the dynamic interactions of TME features is paramount to our understanding of tumour biology and could have significant clinical applications. Hence, there remains an unmet clinical need for validated imaging biomarkers of the TME that can be measured cost-effectively at high spatial and temporal resolution. PAI could offer the flexibility to monitor multiple features with one modality using multi-wavelength imaging, providing a more complete picture of the TME.

Photoacoustic imaging

PAI is an emerging imaging modality, currently in clinical trials (Knieling et al., 2017; Steinberg et al., 2019), that could improve our visualisation of the TME. To create an image, the tissue of interest is illuminated with pulses of light, which cause a pressure change when absorbed and generate ultrasound waves that are detected at the tissue surface using one or more detectors (see 'Photoacoustic effect' in Box 1; Fig. 2A) (Beard, 2011; Ntziachristos et al., 2005; Wang and Yao, 2016). A major advantage of PAI is its scalability: by selecting different light sources, ultrasound detectors and scanning methods, it is possible to tune the spatial resolution, temporal resolution, imaging depth and image contrast. Both image spatial resolution and tissue attenuation scale with increasing ultrasound frequency: low-frequency ultrasound detection at a few MHz enables deep-tissue imaging with centimetre penetration and submillimetre resolution, whereas increasing the detection frequency pushes towards micron resolution but compromises the penetration depth. Technical developments in data acquisition and processing speeds will lead to improvements in the temporal resolution, but current state-of-the-art technology can achieve sub-second two-dimensional imaging, and three-dimensional images in seconds to minutes (Beard, 2011; Ntziachristos et al., 2005; Wang and Yao, 2016). To form an image, ultrasound signals must be acquired from different locations, either by

Disease Models & Mechanisms (2019) 12, dmm039636. doi:10.1242/dmm.039636

Table 1. Current imaging techniques for visualising different features of the tumour microenvironment (TME) *in vivo*

Technique	Principle	Advantages	Disadvantages	References
Tumour vasculature and hypoxia				
DCE-CT	Iodinated contrast agents are injected to measure vascular perfusion	• Well-established CT technique • Low cost • Widely available	• Contrast agent can cause toxicity • Ionising radiation • Lack of standardised protocols	Heiken, 2008; Ohno et al., 2014
DCE-MRI	Paramagnetic contrast agents are injected to measure vascular perfusion	• Well-established MRI technique • Widely available • Many gadolinium chelates are approved clinically	• Contrast agent can cause toxicity • High cost of MRI	Alonzi et al., 2007; Ohno et al., 2014; Rogosnitzky and Branch, 2016
BOLD MRI	Measures blood oxygenation using the paramagnetic property of Hb	• Well-established MRI technique • Utilises endogenous contrast • Measurements correlate with tissue oxygenation	• Signal can be confounded by changes in blood volume and flow • Intrinsically low signal • High cost of MRI	Hallac et al., 2014; Hoskin et al., 2007; Howe et al., 2001
OE MRI	T1 relaxation time is inversely proportional to plasma dissolved oxygen. ΔT1 is measured following a breathing gas challenge to measure areas of low and high blood oxygenation	• Oxygen contrast is more rapidly reversible than injectable contrast • Measurements correlate with tissue oxygenation	• Intrinsically low signal • High cost of MRI	Hallac et al., 2014; Howe et al., 2001; O'Connor et al., 2016
FMISO-PET	An injected radiolabelled nitroimidazole derivative accumulates in hypoxic areas	• FMISO has the potential to give a direct quantification of tissue hypoxia • Can be used to trace metabolic processes	• Long uptake time of tracers such as FMISO leads to poor SNR in tumour • Radioactive isotope administration • Intrinsically low resolution of PET (~5 mm)	Lopci et al., 2014
EF5-PET	An injected radiolabelled nitroimidazole derivative accumulates in hypoxic areas	• More stable than FMISO • Possible correlation to outcome	• Limited experimental evidence compared to FMISO • More complicated labelling chemistry compared to FMISO • Radioactive isotope administration • Intrinsically low resolution of PET (~5 mm)	Koch and Evans, 2015; Lopci et al., 2014
$H_2^{15}O$- PET	Radioactive water is injected to measure vascular perfusion	• Short half-life of ^{15}O enables serial measurements in a single scan	• Short half-life of ^{15}O limits application to sites with an on-site cyclotron • Radioactive isotope administration • Intrinsically low resolution of PET (~5 mm)	van der Veldt et al., 2010
DCE- ultrasound	Microbubbles are injected to generate differences in acoustic impedance with the surrounding tissue, to measure perfusion	• Low cost • High resolution (~100 μm to 1 mm) • Increased SNR compared to conventional ultrasound	• Contrast agent can cause toxicity • Ultrasound limited to localised imaging	Heiken, 2008; Saini and Hoyt, 2014
Doppler ultrasound	Utilises the Doppler effect to image the movement of fluids (e.g. blood) and measure their direction and velocity	• Low cost • Widely available • Allows for serial measurements of blood flow and perfusion without a contrast agent • Easy to combine with other ultrasound techniques	• Challenging to detect motion in small, deep vessels • Cannot distinguish signal arising from individual or aggregated erythrocytes • Ultrasound limited to localised imaging	Fleischer, 2000; Gee et al., 2001; Postema et al., 2015; Sehgal et al., 2000; Xu et al., 2017

Continued

Table 1. Continued

Technique	Principle	Advantages	Disadvantages	References
DOSI	Utilises the distinct spectra of Hb and HbO_2 to visualise blood haemoglobin concentration and oxygenation	• Utilises endogenous contrast • Fast acquisition • Allows visualisation of multiple TME features through spectral separation	• Low resolution (~1 cm) at depths at or above 1 cm due to strong attenuation and scattering of diffuse light in tissue	Cerussi et al., 2006; Di Leo et al., 2017; Tromberg et al., 2005
Intravital microscopy	An intravascular fluorescent contrast agent is injected to enable optical microscopy of tumour vasculature in a living animal through surgical procedures	• Micron resolution visualisation of capillary networks	• Invasive • Challenging to apply clinically • Small field of view • Depth limit of ~1 mm due to strong attenuation and scattering of diffuse light in tissue	Michiels et al., 2016; Ramamonjisoa and Ackerstaff, 2017
PAI	Utilises the distinct spectra of Hb and HbO_2 to visualise blood haemoglobin concentration and oxygenation	• Higher penetration depth compared to other optical techniques • Utilises endogenous contrast • Fast acquisition • Good technical and biological validation of haemoglobin measurements • Low cost • Easy to implement into existing ultrasound systems • Allows visualisation of multiple TME features through spectral separation	• PAI limited to localised imaging • Difficult to quantify and resolve chromophores with current reconstruction and processing algorithms	Beard, 2011; Brochu et al., 2017; Cox et al., 2012; Diot et al., 2017; Ntziachristos et al., 2005; Wang and Hu, 2012; Wang and Yao, 2016
Tumour fibrosis				
DCE-CT	Delayed-enhancement after iodinated contrast agent injection can reveal fibrotic tissue	• Well-established CT technique • Low cost • Widely available	• Contrast agent can cause toxicity • Ionising radiation • Lack of standardised protocols for fibrosis assessment • Not specific to fibrosis: delayed enhancement can be confounded by oedema and necrosis	Heiken, 2008; Koyasu et al., 2016; Ohno et al., 2014; Qureshi et al., 2016
DW-MRI	Utilises the diffusion of water molecules to generate contrast in MR images to calculate an apparent diffusion coefficient that can relate to fibrosis	• Well-established MRI technique • Widely available	• Signal can be confounded by tumour cell necrosis • Motion interferes with signal • High cost of MRI	Muzard et al., 2009; Taouli et al., 2007
Ultrasound elastography	Measures tissue stiffness by analysing tissue strain under stress (compression) or by imaging shear waves, whose propagation is governed by tissue stiffness	• Low cost • Can image deep organs • Ease of use	• Not specific to fibrosis: can be confounded • Compression-based methods depend on operator, leading to reproducibility issues • Ultrasound limited to localised imaging	Muzard et al., 2009; Talwalkar et al., 2007
MRI elastography	Uses a specialist MR sequence to measure the wavelength of applied mechanical shear waves as they propagate through tissue, which is governed by tissue stiffness	• Imaging not influenced by presence of ascites and obesity, which limit the use of ultrasound elastography • Can be implemented into a conventional MRI system with a few hardware and software modifications	• May require patient to repeatedly hold their breath, to reduce motion artefacts • When imaging liver tissue, excess iron decreases the SNR • High cost of MRI	Akkaya et al., 2018; Venkatesh et al., 2008

Continued

Table 1. Continued

Technique	Principle	Advantages	Disadvantages	References
Intravital microscopy	Uses collagen second harmonic generation for optical microscopy in a living animal through surgical procedures	• Micron resolution visualisation of collagen fibres	• Invasive • Challenging to apply clinically • Small field of view • Depth limit of ∼1 mm due to strong attenuation and scattering of diffuse light in tissue	Ramamonjisoa and Ackerstaff, 2017
PAI	Utilises the endogenous optical contrast of collagen	• Higher penetration depth compared to other optical techniques • Utilises endogenous contrast • Fast acquisition • Low cost • Easy to implement into existing ultrasound systems • Allows visualisation of multiple TME features through spectral separation	• PAI limited to localised imaging • Difficult to quantify and resolve chromophores with current reconstruction and processing algorithms • Lack of technical and biological validation of collagen imaging • At wavelengths above 1000 nm, water absorption increases dramatically, limiting sensitivity to other absorbing species	Lei et al., 2016; Zhu et al., 2018
MRI	Uses specific fat-detection-imaging MR sequences to provide lipid-weighted images of soft tissue	• Utilises the intrinsic excellent soft-tissue contrast of MRI • Many available imaging sequences are available, which provides flexibility • Widely available	• High cost of MRI • Lack of standardised data-acquisition protocols	Pokharel et al., 2013
Tumour lipid content				
[1-^{11}C]acetate-PET	Injected radiolabelled acetate is incorporated via *de novo* lipogenesis to monitor the rate of fatty acid synthesis	• Promising alternative metabolic tracer, particularly for identifying metastases	• The short half-life of [1-^{11}C]acetate limits application to sites with an on-site cyclotron • Acetate accumulates in normal tissues, leading to high background • Radioactive isotope administration • PET has intrinsically low resolution (∼5 mm)	Lewis et al., 2014; Schöder and Larson, 2004
PAI	Utilises the endogenous optical absorption of lipids	• Higher penetration depth compared to other optical techniques • Utilises endogenous contrast • Fast acquisition • Low cost • Easy to implement into existing ultrasound systems • Allows visualisation of multiple TME features through spectral separation	• PAI limited to localised imaging • Difficult to quantify and resolve chromophores with current reconstruction and processing algorithms • Lack of technical and biological validation of lipid imaging with PAI • At wavelengths above 1000 nm, water absorption increases dramatically, limiting sensitivity to other absorbing species	Cao et al., 2018; Diot et al., 2017; Jansen et al., 2014; Wang et al., 2012; Wilson et al., 2014; Wu et al., 2015
CT	Monitors anatomical changes in tumour size associated with changing immune cell infiltrate	• Good soft-tissue contrast and anatomical imaging • Low cost • Widely available	• Ionising radiation • Anatomical images do not provide molecular information, such as the subtype of immune cells infiltrating	Nishino et al., 2018

Continued

Table 1. Continued

Technique	Principle	Advantages	Disadvantages	References
Immune cell infiltration				
^{18}F-FDG PET	Injected radiolabelled glucose is avidly taken up in identify infiltrating inflammatory cells	• FDG-PET has been widely used to identify and monitor inflammatory diseases	• Produces false-positive results when used post-surgery or post-biopsy due to surgically induced inflammation • Produces false-negative results if tumour is close to sites of physiological uptake such as kidney and liver • Cancer cells also have increased glucose metabolism: not specific to inflammatory immune cells • Radioactive isotope administration • PET has intrinsically low resolution (~5 mm)	Hammoud, 2016; Kostakoglu et al., 2003; Wu et al., 2013
Intravital microscopy	Immune cells are fluorescently labelled or express genetic reporters to enable optical microscopy of tumour immune cell infiltrate locally in a living animal through surgical procedures	• Single-cell resolution for monitoring cell-cell interactions	• Invasive • Challenging to apply clinically • Small field of view • Depth limit of ~1 mm due to strong attenuation and scattering of diffuse light in tissue	Arina et al., 2016; Hanna et al., 2016; Ramamonjisoa and Ackerstaff, 2017
PAI	Immune cells are labelled with an exogenous contrast agent or express genetic reporters	• Higher penetration depth compared to other optical techniques • Fast acquisition • Low cost • Easy to implement into existing ultrasound systems • Allows visualisation of multiple TME features through spectral separation, with one modality	• PAI limited to localised imaging • Difficult to quantify and resolve chromophores with current reconstruction and processing algorithms • Limited sensitivity due to the limited number of signalling molecules that can be labelled per cell	Brunker et al., 2017; Filippi et al., 2018; Tzoumas et al., 2014; Yin et al., 2018; Zheng et al., 2018
Radiolabelled antibodies in PET	Injected radiolabelled antibodies target whole-body tracking of immune cell populations and signalling molecules	• Correlation with outcome • Antigen specificity • Ease of production	• May lack tumour penetrance • Can negatively impact T-cell effector functions • Radioactive isotope administration • PET has intrinsically low resolution (~5 mm)	Gibson et al., 2018; Larimer et al., 2016; Larimer et al., 2017; Maute et al., 2015; Natarajan et al., 2017; Tavaré et al., 2014

BOLD, blood oxygen level dependent; CT, computed tomography; DCE, dynamic contrast-enhanced; DOSI, diffuse optical spectroscopic imaging; DW, diffusion-weighted; ^{18}F-FDG, 2-deoxy-2-18F-fluoro-D-glucose; FMISO, fluoromisonidazole; Hb, deoxyhaemoglobin; HbO2, oxyhaemoglobin; MRI, magnetic resonance imaging; OE, oxygen enhanced; PAI, photoacoustic imaging; PET, positron emission tomography; SNR, signal-to-noise ratio.

scanning a single detector over the region of interest or by employing a detector array, and then these signals can be naively backprojected (beamformed) or subjected to more complex reconstruction algorithms to improve image quality (Beard, 2011).

Photoacoustic image contrast arises due to optical absorption, which results in ultrasound generation. When using near-infrared wavelengths of light (620-950 nm) for illumination, several vital endogenous molecules for the TME strongly absorb light (Fig. 2B). Using only endogenous contrast and acquiring data at multiple wavelengths, PAI can therefore non-invasively visualise vascular morphology, blood oxygenation, fibrosis and lipid content simultaneously with a single technique. Other features, such as immune cell infiltration, can be imaged by introducing targeted exogenous contrast agents or *in-vitro*-labelled immune cells, allowing a complete picture of the dynamic relationships in the TME to be revealed with a single technique. Such contrast agents, either injected externally, taken up by cells (Weber et al., 2016) or expressed in genetically modified cells (Brunker et al., 2017), work by providing additional sources of optical absorption with distinct spectra; the contrast agent is typically bound to, or expressed by, a targeting component in order to highlight specific structural or functional tissue features. PAI with exogenous contrast agents remains subject to the same spatial resolution and penetration depth trade-off as imaging of endogenous molecules; in addition, it is

Disease Models & Mechanisms (2019) 12, dmm039636. doi:10.1242/dmm.039636

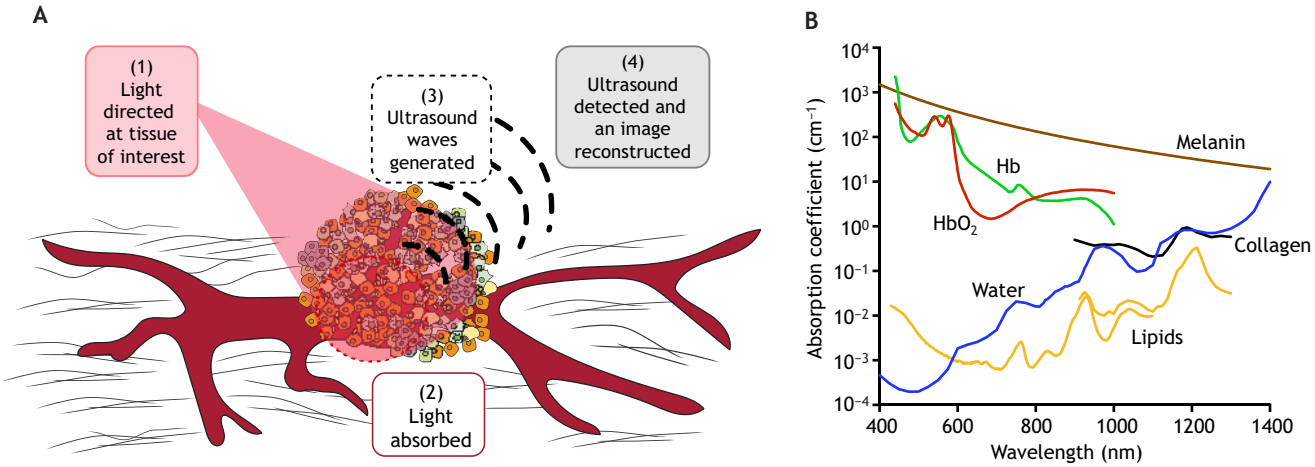

Fig. 2. Principles of photoacoustic imaging (PAI). (A) During PAI, pulses of light illuminate the tissue (1). When light is absorbed (2), a transient heating gives rise to ultrasound waves (3). The ultrasound waves are then detected and used to reconstruct an image of the optical absorption in tissue (4). (B) Absorption spectra of endogenous molecules that absorb light pulses and can provide insight into the tumour microenvironment (TME). Panel B is reproduced with permission from Weber et al. (2016). This image is not published under the terms of the CC-BY licence of this article. For permission to reuse, please see Weber et al. (2016). Hb, deoxyhaemoglobin; HbO_2, oxyhaemoglobin.

important to select a signalling compound with distinct absorption peaks and strong optical absorption above 600 nm, thus avoiding signal corruption by endogenous molecules (Fig. 2B).

Compared to existing optical techniques such as DOSI and intravital microscopy, PAI maintains high spatial resolution to a greater imaging depth due to the detection of ultrasound waves, which scatter less than light in tissue. By utilising optical absorption and contrast, PAI maintains high molecular specificity (Beard, 2011; Ntziachristos et al., 2005; Wang and Yao, 2016) compared to standard ultrasound techniques (Table 1). Additionally, many TME features can be detected simultaneously with PAI due to the multi-wavelength data acquisition, without administration of a contrast agent or radioactive agent. Despite the ability of PAI to image beyond the optical diffusion limit (Box 1), it has limited penetration depth compared to clinical whole-body modalities such as MRI, PET and CT. Preclinically, PAI is frequently used as a whole-body imaging modality, but this is not possible clinically, where the depth limits of PAI are approached. Introducing PAI through endoscopes can lift this limitation to some extent, but PAI would not compete with whole-body modalities such as PET for disease staging in patients (Table 1). Nonetheless, in tumours growing within the depth-detection limits of PAI, such as in the breast, PAI could follow initial conventional diagnostic imaging with MRI or ultrasound to provide additional insight into the TME. It is worth noting that combining imaging in a multi-modal approach would allow the limitations of one technique to be compensated for by another, and it is likely that PAI will be used in this way, for example by combining PAI with ultrasound (Bar-Zion et al., 2016; Diot et al., 2017; Neuschler et al., 2018). For the remainder of this Review, we will discuss how PAI has been used so far to image the TME, some of the challenges currently faced, and its potential for preclinical and clinical application in oncology.

Photoacoustic imaging of vasculature and oxygenation

Preclinical PAI in small animal models allows detailed tumour vascular architecture and morphology to be visualised non-invasively over time at sub-100-µm resolution using just a single wavelength of light, commonly selected as an isosbestic point (Box 1) of Hb and HbO_2 (e.g. 532 nm). This method has been used to monitor the developing vasculature in early tumours, showing changes in structure such as increased tortuosity (Fig. 3A) (Laufer et al., 2012), diameter and density (Lao et al., 2008), as well as the recruitment of existing vessels to feed the tumour mass (Laufer et al., 2012; Omar et al., 2015). Imaging biomarkers such as blood volume and vessel connectivity could be extracted from these images, but the majority of studies to date did not include quantification. Nonetheless, they show how PAI can provide high-resolution visualisation of the development of tumour vasculature at depths of several centimetres.

Alternatively, utilising the differential absorption spectra of Hb and HbO_2 (Fig. 2B), PAI data can be recorded at multiple wavelengths and subjected to spectral unmixing algorithms to calculate imaging biomarkers related to total haemoglobin concentration ($THb=Hb+HbO_2$) and blood oxygen saturation ($sO_2=HbO_2/THb$). These functional parameters can provide further insight into the TME, as detailed below.

PAI THb tends to be higher in tumours compared to normal tissue (Chekkoury et al., 2016; Li et al., 2008; Raes et al., 2016) because of increased angiogenesis, and also tends to be concentrated around the periphery as the cell line models used, such as melanoma cell-line-derived xenografts (Lavaud et al., 2017), tend to be less vascularised in their core. One study demonstrated a decrease in THb as the tumour developed (Imai et al., 2017), showing that this parameter may be context-dependent and that PAI can sensitively resolve such differences.

PAI generally measures lower sO_2 values in tumours compared to normal tissue (Chekkoury et al., 2016; Imai et al., 2017; Lavaud et al., 2017; Li et al., 2008; Raes et al., 2016), consistent with poor perfusion and/or high consumption of O_2 from the blood due to tumour hypoxia. A recent study in breast cancer models demonstrated that sO_2 measurements correlated with vascular maturity, measured by pericyte coverage of vessels *ex vivo* (Quiros-Gonzalez et al., 2018). Altering the gas delivered to the mouse from air to 100% oxygen and measuring the change in sO_2 can distinguish between well-perfused (with high ΔsO_2) and poorly perfused (with low ΔsO_2) prostate cancer models (Fig. 3B) (Bendinger et al., 2018; Tomaszewski et al., 2017). Importantly, low sO_2 and ΔsO_2 spatially correlate with regions of tissue hypoxia and necrosis (Gerling et al., 2014; Tomaszewski et al., 2018). In the

Disease Models & Mechanisms (2019) 12, dmm039636. doi:10.1242/dmm.039636

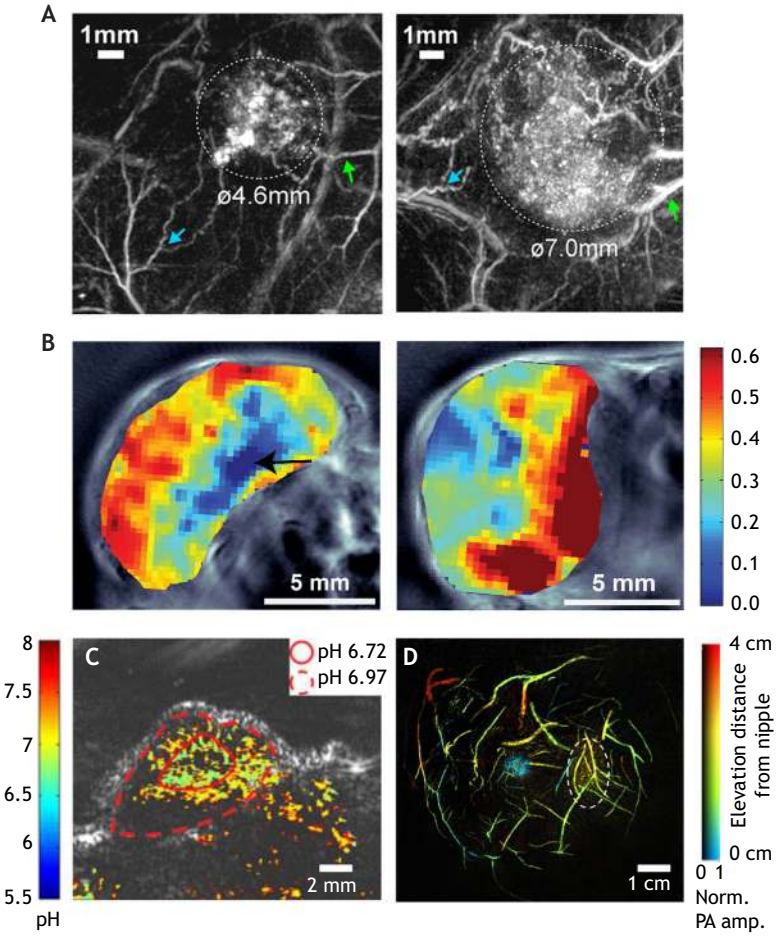

Fig. 3. Example photoacoustic images of the vasculature. (A) Shown are *x-y* maximum intensity projections of a human colorectal tumour (SW1222) and the surrounding vasculature between day 7 and day 8 post-inoculation. Dashed white lines indicate tumour margins. Green arrows show common vascular features between images. Increasing tortuosity of normal blood vessels between day 7 and 8 is indicated by blue arrows. Reproduced with permission from Laufer et al. (2012) and the *Journal of Biomedical Optics*. This image is not published under the terms of the CC-BY licence of this article. For permission to reuse, please see Laufer et al. (2012). (B) Representative images of PC3 (left) and LNCaP (right) tumours showing the spatial distribution of ΔsO_2 measured using PAI at multiple wavelengths. PC3 tumours displayed lower ΔsO_2 compared to LNCaP tumours and had a core with low ΔsO_2 (black arrow). Reproduced with minor formatting changes from Tomaszewski et al. (2017). (C) Photoacoustic pH image of rat glioma tumours at 75 min after SNARF-5F nanoparticle injection. The pH in the centre area (i.e. the area within the solid line) and the peripheral areas (i.e. the area between the solid line and the dashed line) are averaged, respectively. Reproduced with minor formatting changes from Jo et al. (2017). (D) Depth-encoded PAI images of the breast acquired while the patient, a 49-year-old woman with a stromal fibrosis or fibroadenoma, held her breath. Dashed white lines indicate tumour margin. Reproduced with minor formatting changes from Lin et al. (2018).

same studies, vascular perfusion was measured *in vivo* using Indocyanine Green, a clinically approved near-infrared dye. In general, functional PAI studies have focussed on blood flow (van den Berg et al., 2015) rather than perfusion, and measuring blood flow at clinically relevant depths has proved to be challenging (Brunker and Beard, 2016) due to a poor velocity signal-to-noise ratio (SNR). However, it is possible that alternative approaches (for example, speckle tracking) could provide semi-quantitative flow/perfusion information that, combined with measures of blood oxygenation, could indicate the level of oxygen delivery to the tumour.

PAI biomarkers relating to vascular function have also been used to predict and monitor treatment response in preclinical cancer models. A decrease in THb and a corresponding increase in HbO_2 has been seen in ovarian mouse tumour models following anti-angiogenic therapies, indicating vessel normalisation, which was shown *ex vivo* by an increase in pericyte coverage of vessels and decreased vessel density (Bohndiek et al., 2015). High tumour sO_2 was demonstrated to be an early biomarker of radiotherapy response (Rich and Seshadri, 2016) and could predict which tumours would respond to radiotherapy in mouse models of head and neck cancer (Costa et al., 2018). These studies demonstrate the potential of PAI in predicting and monitoring tumour response, which could assist with patient stratification and inform therapeutic strategies.

Exogenous contrast agents can also be used to assess metabolic changes in the hypoxic TME. Amine-oxide probes can give a direct measure of tissue hypoxia (Knox et al., 2017), complementing the assessment of vascular features with endogenous PAI. The pH can be evaluated (Chen et al., 2015) using ratiometric changes in the optical absorption coefficient of a given probe (Chatni et al., 2011; Jo et al., 2017), allowing visualisation of the acidic pH of the TME (Fig. 3C), particularly in the tumour core (Jo et al., 2017). The ability to image several of these features within a single tumour simultaneously, by acquiring data at multiple wavelengths, is one of the unique advantages of PAI that could yield tremendous insight into the dynamic TME interactions.

In a clinical context, application of PAI to monitor vascular features of the TME have focussed on breast cancer, where PAI can be combined with existing ultrasound imaging approaches. Hand-held PAI probes, similar to existing ultrasound probes, have been used in clinical trials to demonstrate higher THb in tumours compared to normal tissue (Diot et al., 2017) and an increase in abnormal features such as vessels radiating from the tumour mass (Neuschler et al., 2018). Similar to standard X-ray mammography, the Twente photoacoustic mammoscope compresses the breast between a glass window and a flat ultrasound transducer matrix (Manohar et al., 2005). This system identified malignant lesions that displayed high PA contrast independent of breast density (Heijblom et al., 2016), but specificity remains a concern (Heijblom et al., 2016). Bespoke hemispherical transducer arrays, which form a cup that surrounds the whole human breast, have also been developed. These systems have become highly sophisticated in recent years, revealing the detailed vessel networks in the breast (Kruger et al., 2016; Lin et al., 2018; Toi et al., 2017; Yamaga et al., 2018). A pivotal study recently demonstrated that, when the patient holds their breath during the scan, thereby decreasing motion artefacts, detailed vascular features can be resolved to a depth of up to 4 cm

(Fig. 3D) (Lin et al., 2018). These studies demonstrate how PAI could be utilised to diagnose and stage breast cancers based on vascular TME features.

Photoacoustic imaging of the ECM and lipid composition

To date, the application of PAI to detect fibrosis and lipids *in vivo* has been focused mainly on diseases beyond cancer, such as Crohn's disease (Lei et al., 2016; Zhu et al., 2018) and atherosclerosis (Cao et al., 2018; Jansen et al., 2014; Wang et al., 2012; Wu et al., 2015); however, early studies show promise for its application in the TME.

In preclinical studies of chronic fibrotic diseases such as Crohn's disease, collagen content has been probed at wavelengths above 1000 nm to detect fibrotic disease in *ex vivo* and *in vivo* rat intestine (Lei et al., 2016; Zhu et al., 2018), with results correlating to histological analyses. In a pivotal PAI clinical trial of 108 patients, active and non-active Crohn's disease was distinguished by measuring THb levels in the intestinal wall, bypassing the need to visualise collagen directly (Knieling et al., 2017). In a preclinical model of liver fibrosis, the PAI signal was higher in fibrotic livers compared to control livers, although the individual contributions of collagen, haemoglobin and possibly other chromophores to the signal could not be determined with the single 808 nm wavelength used in this study (van den Berg et al., 2016). Visualising collagen with PAI is challenging, as light above 1000 nm will be absorbed by lipids, water and collagen in the skin, ultimately leading to a decreased signal from deeper tissues (Zhu et al., 2018), which may explain the lack of clinical studies to date. To enable clinical translation, the application of depth- and wavelength-dependent light fluence (Box 1) correction models could be evaluated, although the application of these models *in vivo* remains challenging due to limited knowledge of the spatial distribution of optical parameters in living tissue (Brochu et al., 2017; Cox et al., 2012). Alternative methods of light delivery directly to the tumour site using fibre optics may also circumvent such challenges with minimally invasive rather than completely non-invasive imaging.

Monitoring the production or activity of MMPs in the TME could provide a diagnostic or predictive biomarker of metastasis and has also been achieved with PAI using exogenous contrast agents (Dragulescu-Andrasi et al., 2013; Levi et al., 2013; Yin et al., 2019). The production of MMPs has been monitored preclinically, with a probe cleaved by MMP-2 and MMP-9 giving an increase in PAI signal upon cleavage in preclinical models of follicular thyroid carcinoma (Levi et al., 2013), which express high levels of MMP-2, MMP-7 and MMP-9 compared to benign thyroid adenomas. Recently, a similar PAI probe design was also shown to quantify MMP-2 expression in mouse mammary tumours (Yin et al., 2019). Given the many roles of MMPs in tumour development and progression (Egeblad and Werb, 2002), monitoring their production and activity *in vivo* is of interest.

PAI of lipids has been mainly applied to monitor atherosclerotic plaques using an intravascular-imaging catheter in either rabbit aorta or *ex vivo* human coronary arteries (Cao et al., 2018; Jansen et al., 2014; Wang et al., 2012; Wu et al., 2015), although these studies lack quantification. Nonetheless, using the catheter bypasses the issue of absorption of light above 1000 nm in the skin, allowing visualisation of lipid distribution in the vessel wall. Single-wavelength imaging visualised relative lipid content in diseased and non-diseased states (Cao et al., 2018; Wang et al., 2012), whereas dual- or multi-wavelength imaging identified cholesterol derivatives in the plaques (Jansen et al., 2014; Wu et al., 2015). This methodology could also be used to monitor lipid content in tumours that can be accessed endoscopically, such as colorectal cancer, which has been shown to be driven by fatty acid synthesis pathways (Zhan et al., 2008).

As mentioned earlier, lipids play a vital role in the breast TME. In transgenic mice, *in vivo* multi-wavelength PAI has demonstrated a decrease in lipid content with increasing tumour stage (Fig. 4A), presumably as fatty structures in the breast are replaced with fibrotic structures (Wilson et al., 2014). The clinical potential of lipid PAI in breast cancer has been demonstrated using a hand-held multispectral optoacoustic tomography probe. This study showed that lipid structures nearby tumours were disrupted, perhaps as tumours invaded the surrounding healthy adipose tissue (Diot et al., 2017). Additionally, signals attributed to lipids were higher in larger tumours compared to smaller ones, but how this affected the biology of these patients' tumours remains to be elucidated (Diot et al., 2017).

Photoacoustic imaging of immune cell infiltration

Exogenous contrast agents can theoretically label any cell type of interest and track these cells in the TME. Strong absorbers with little or no fluorescence provide the best contrast because the absorbed energy can be converted efficiently into ultrasound signals rather than being re-emitted as fluorescence. Fluorophores with a low-quantum yield have also proved successful in providing photoacoustic contrast. Fluorescently labelled T cells were first imaged with PAI *ex vivo* (Tzoumas et al., 2014). Since then, exogenous T-cell migration into subcutaneous tumours *in vivo* was monitored with PAI after labelling with a near-infrared fluorescent dye (Fig. 4B) (Zheng et al., 2018). This is one of the first reports of immune cell tracking with PAI and demonstrates the capability of PAI to longitudinally monitor immune cells in the TME at depths beyond the optical diffusion limit (Box 1). Organic nanoparticles and small-molecule dyes have been used as contrast agents to label and track injected stem cells *in vivo* with PAI (Filippi et al., 2018; Yin et al., 2018), a method that could be applied to numerous cell types (Meir et al., 2014; Weber et al., 2016). Such pre-loading of cells with nanoparticles avoids macrophage phagocytosis, which is an issue with systemic delivery of nanoparticles (Weber et al., 2016). In addition to cell labelling, the use of PAI with genetic reporters has expanded (Brunker et al., 2017). For example, cancer cells engineered to produce eumelanin via tyrosinase reporter expression allowed detailed 3D imaging of tumour growth *in vivo* (Jathoul et al., 2015). The extent to which this more invasive genetic approach would be tolerated by the immune system in a clinical setting has yet to be established. Another challenge with reporter genes is the interference of background signal from endogenous chromophores such as haemoglobin, which could be overcome with the use of photoswitchable proteins whose absorption spectra changes upon illumination with a specific wavelength (Yao et al., 2015). Reporter gene technology could be applied to track immune cells in the future (Brunker et al., 2017).

Conclusions

We have moved into an age of cancer biology research where tumours are considered not as isolated masses of cancer cells but as 'organs' with multiple cell types supporting growth and development. The complex contribution of the TME to tumour evolution is now well recognised as influencing cancer cell gene expression, growth, survival, motility, local invasion and metastasis. There are also dynamic interactions between different TME features that regulate processes such as blood vessel outgrowth that we are just beginning to understand.

Given the importance of the TME in tumour development and progression, it is surprising that our ability to image TME features is

Disease Models & Mechanisms (2019) 12, dmm039636. doi:10.1242/dmm.039636

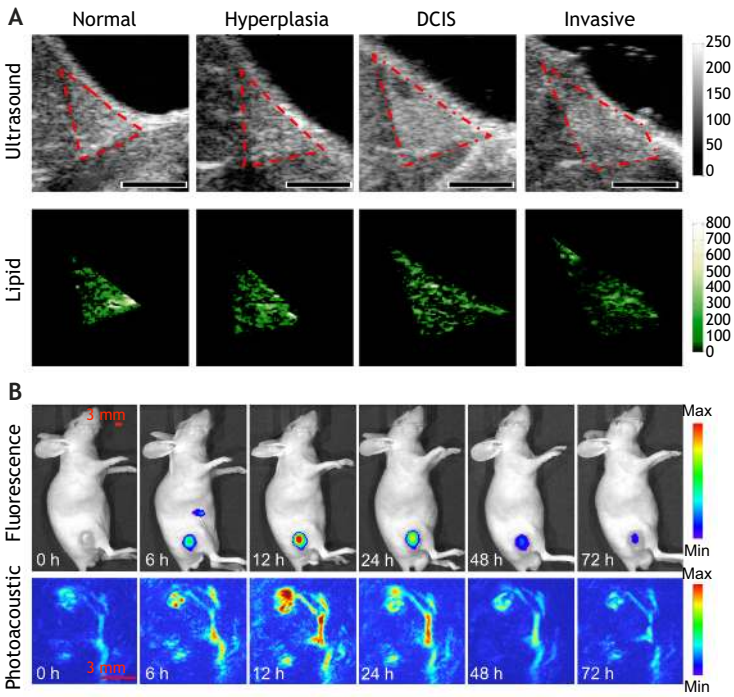

Fig. 4. Example photoacoustic images of lipid content and immune cell tracking. (A) Representative transverse B-mode ultrasound images (top row) and PAI performed at multiple wavelengths to reveal lipid content (bottom row) of four histologies [normal, hyperplasia, ductal carcinoma *in situ* (DCIS) and invasive carcinoma] from distinct animals of a transgenic mouse model of breast cancer progression. Lesion severity increases from left to right. Regions of interest are outlined in red on B-mode images. Scale bars: 2 mm. Reproduced with minor formatting changes from Wilson et al. (2014). (B) *In vivo* imaging of near-IR-797-labelled T cells in a mouse sarcoma model displaying infiltration of T cells over time with a peak at 12 h and subsequent decline up until 72 h post-adoptive transfer. Copyright Wiley-VCH Verlag GmbH & Co. KGaA. Reproduced from Zheng et al. (2018) with permission, with minor formatting changes. This image is not published under the terms of the CC-BY licence of this article. For permission to reuse, please see Zheng et al. (2018).

lacking both in preclinical models and in clinical applications. Many existing imaging modalities have been used to visualise vasculature, hypoxia, fibrosis, lipid synthesis and immune cells (Table 1); however, they tend to carry high cost, require injection of contrast agents, resolve just one feature at a time, and exhibit poor spatial and temporal resolution. PAI is a relatively low-cost modality that has the potential to overcome some of these shortfalls; for example, it can visualise multiple features by acquiring data at multiple wavelengths to separate both endogenous contrast from haemoglobin, collagen and lipids, and visualise injected exogenous contrast agents for features such as acidity, enzyme activity and immune cells, generating a complete picture of the TME. PAI spatial resolution scales with penetration depth, reaching ∼100 µm at ∼3 cm depth, which is advantageous for exploring relationships between the different TME features preclinically.

The studies reviewed here indicate that PAI can inform on TME features in preclinical models and holds promise for clinical translation. Currently, further technical and biological validation of PAI biomarkers is needed to increase uptake of the modality in studies of TME biology or clinical evaluation of TME features (Waterhouse et al., 2019). In terms of technical validation, some studies have reported on standardisation of data acquisition and analysis (Abeyakoon et al., 2018; Bohndiek et al., 2013; Joseph et al., 2017; Martinho Costa et al., 2018; Neuschmelting et al., 2016). Establishing precise and accurate PAI biomarker measurements will provide confidence, while development of standardised stable test objects, or 'phantoms', that can be applied in a multi-centre setting is vital for routine quality assurance and control (O'Connor et al., 2017). Additionally, correcting for spectral distortions of illumination light as it passes through tissue would allow absolute quantification of optically absorbing molecules, but remains a significant challenge to apply *in vivo* and hence is an active area of research in the field (Brochu et al., 2017; Cox et al., 2012).

In terms of biological validation, the extensive use of cell-line-derived cancer models in PAI studies limits the clinical applicability of the work due to the stark genomic and phenotypic differences between clonal cell lines and patient samples (Choi et al., 2014). More clinically relevant models, such as patient-derived xenografts, are gaining popularity (Bruna et al., 2016), although the use of immunocompromised mice limits studies of the immune infiltrate in the TME and of the regulation of angiogenesis by immune cells (De Palma et al., 2017). Humanising the immune system of immunocompromised mice is underway in many laboratories (Morton et al., 2016; Shultz et al., 2007), and applying PAI in these more advanced models would help to advance the imaging modality. Further insights can be obtained by correlating *in vivo* PAI data with other well-validated *in vivo* imaging methods as well as *ex vivo* analyses such as immunohistochemistry and biochemical assays. In the few studies where this has been achieved preclinically, PAI provided *in vivo* biomarkers of vascular maturity and function that correlate with hypoxia (Gerling et al., 2014; Quiros-Gonzalez et al., 2018; Tomaszewski et al., 2017). Additionally, validation of photoacoustic mammography in patients showed an *in vivo* distribution of haemoglobin signal that had good colocalisation with DCE-MRI and correspondence with vascular patterns measured *ex vivo* (Heijblom et al., 2015).

Most clinical studies discussed in this Review are observational and/or conducted in a limited number of patients (Diot et al., 2017; Heijblom et al., 2016; Kruger et al., 2016; Lin et al., 2018; Toi et al., 2017; Yamaga et al., 2018). Their purpose was to investigate how PAI biomarkers could be used in disease diagnosis or assessment of disease severity, for example in differentiation between benign and malignant disease. The best-developed application in this regard, including multi-centre studies, is in breast cancer. PAI could be easily combined with ultrasound imaging, which is conventionally used in breast cancer patient management. PAI has been demonstrated to accurately downgrade benign masses (Menezes et al., 2018; Neuschler et al., 2018) with higher specificity than ultrasound imaging (Neuschler et al., 2018), which could reduce unnecessary biopsies and follow-up appointments, reducing patient distress and healthcare costs. As yet, PAI has not been used in

clinical decision-making and the results of these studies did not affect the diagnostic pathways of the patients involved; radiologists interpreting the photoacoustic images were blinded to the rest of the diagnostic work-up. Other superficial malignancies could also be monitored with PAI. For example, high-resolution PAI is capable of visualising microvasculature in human skin and could be applied to monitor the pathological neovascularisation of melanoma (Hindelang et al., 2019; Omar et al., 2015). Photoacoustic endoscopy is expanding, bypassing limitations in the penetration depth, so could be used to monitor angiogenesis in gastrointestinal tract cancers or cervical cancer with further technological advances (Li et al., 2018; Qu et al., 2018; Yoon and Cho, 2013). Large-scale clinical trials are also being planned for inflammatory conditions (Knieling et al., 2017).

To conclude, PAI can visualise multiple TME features with a single modality; high spatiotemporal resolution, low cost, use of non-ionising radiation and non-invasive properties with potentially easy integration into existing ultrasound systems make PAI an attractive option for monitoring dynamic TME features not only in a preclinical setting but also throughout a patient's treatment regime, from diagnosis and staging to monitoring treatment response.

Competing interests

S.E.B. has received research support from iThera Medical and PreXion Inc., vendors of photoacoustic imaging instruments.

Funding

The authors are funded by Cancer Research UK (C14303/A17197, C47594/A16267, C197/A16465), Engineering and Physical Sciences Research Council (EPSRC; EP/R003599/1) and the Wellcome Trust (204845/Z/16/Z).

References

Abadjian, M.-C. Z., Edwards, W. B. and Anderson, C. J. (2017). Imaging the tumor microenvironment. In *Tumor Immune Microenvironment in Cancer Progression and Cancer Therapy* (ed. P. Kalinski), pp. 229-257. Cham: Springer International Publishing.

Abeyakoon, O., Morscher, S., Dalhaus, N., Ford, S. J., Mendichovszky, I. A., Manavaki, R., Wallis, M., Moyle, P., Woitek, R., Patterson, A. et al. (2018). Optoacoustic imaging detects hormone-related physiological changes of breast parenchyma TT - Optoakustische Bildgebung detektiert physiologische Veränderungen des Brustparenchyms in Abhängigkeit von Zyklusphasen. *Ultraschall. Med.* doi:10.1055/a-0628-6248

Ahmad, M., Long, J. S., Pyne, N. J. and Pyne, S. (2006). The effect of hypoxia on lipid phosphate receptor and sphingosine kinase expression and mitogen-activated protein kinase signaling in human pulmonary smooth muscle cells. *Prostaglandins Other Lipid Mediat.* **79**, 278-286. doi:10.1016/j.prostaglandins.2006.03.001

Akkaya, H. E., Erden, A., Kuru Öz, D., Ünal, S. and Erden, İ. (2018). Magnetic resonance elastography: basic principles, technique, and clinical applications in the liver. *Diagn. Interv. Radiol.* **24**, 328-335. doi:10.5152/dir.2018.18186

Alonzi, R., Padhani, A. R. and Allen, C. (2007). Dynamic contrast enhanced MRI in prostate cancer. *Eur. J. Radiol.* **63**, 335-350. doi:10.1016/j.ejrad.2007.06.028

Arina, A., Idel, C., Hyjek, E. M., Alegre, M.-L., Wang, Y., Bindokas, V. P., Weichselbaum, R. R. and Schreiber, H. (2016). Tumor-associated fibroblasts predominantly come from local and not circulating precursors. *Proc. Natl. Acad. Sci. USA* **113**, 7551-7556. doi:10.1073/pnas.1600363113

Baenke, F., Peck, B., Miess, H. and Schulze, A. (2013). Hooked on fat: the role of lipid synthesis in cancer metabolism and tumour development. *Dis. Model. Mech.* **6**, 1353-1363. doi:10.1242/dmm.011338

Bar-Zion, A., Yin, M., Adam, D. and Foster, F. S. (2016). Functional flow patterns and static blood pooling in tumors revealed by combined contrast-enhanced ultrasound and photoacoustic imaging. *Cancer Res.* **76**, 4320-4331. doi:10.1158/0008-5472.CAN-16-0376

Beard, P. (2011). Biomedical photoacoustic imaging. *Interface Focus* **1**, 602-631. doi:10.1098/rsfs.2011.0028

Bendinger, A. L., Glowa, C., Peter, J. and Karger, C. P. (2018). Photoacoustic imaging to assess pixel-based sO_2 distributions in experimental prostate tumors. *J. Biomed. Opt.* **23**, 36009-36011. doi:10.1117/1.JBO.23.3.036009

Blomberg, O. S., Spagnuolo, L. and de Visser, K. E. (2018). Immune regulation of metastasis: mechanistic insights and therapeutic opportunities. *Dis. Model. Mech.* **11**, dmm036236. doi:10.1242/dmm.036236

Bohndiek, S. E., Bodapati, S., Van De Sompel, D., Kothapalli, S.-R. and Gambhir, S. S. (2013). Development and application of stable phantoms for the evaluation of photoacoustic imaging instruments. *PLoS ONE* **8**, e75533. doi:10.1371/journal.pone.0075533

Bohndiek, S. E., Sasportas, L. S., Machtaler, S., Jokerst, J. V., Hori, S. and Gambhir, S. S. (2015). Photoacoustic tomography detects early vessel regression and normalization during ovarian tumor response to the anti-angiogenic therapy Trebananib. *J. Nucl. Med.* **56**, 1942-1947. doi:10.2967/jnumed.115.160002

Bonnans, C., Chou, J. and Werb, Z. (2014). Remodelling the extracellular matrix in development and disease. *Nat. Rev. Mol. Cell Biol.* **15**, 786. doi:10.1038/nrm3904

Bordeleau, F., Mason, B. N., Lollis, E. M., Mazzola, M., Zanotelli, M. R., Somasegar, S., Califano, J. P., Montague, C., LaValley, D. J., Huynh, J. et al. (2017). Matrix stiffening promotes a tumor vasculature phenotype. *Proc. Natl. Acad. Sci. USA* **114**, 492-497. doi:10.1073/pnas.1613855114

Britto, D. D., Wyroba, B., Chen, W., Lockwood, R. A., Tran, K. B., Shepherd, P. R., Hall, C. J., Crosier, K. E., Crosier, P. S. and Astin, J. W. (2018). Macrophages enhance Vegfa-driven angiogenesis in an embryonic zebrafish tumour xenograft model. *Dis. Model. Mech.* **11**, dmm035998. doi:10.1242/dmm.035998

Brochu, F. M., Brunker, J., Joseph, J., Tomaszewski, M. R., Morscher, S. and Bohndiek, S. E. (2017). Towards quantitative evaluation of tissue absorption coefficients using light fluence correction in optoacoustic tomography. *IEEE Trans. Med. Imaging* **36**, 322-331. doi:10.1109/TMI.2016.2607199

Bruna, A., Rueda, O. M., Greenwood, W., Batra, A. S., Callari, M., Batra, R. N., Pogrebniak, K., Sandoval, J., Cassidy, J. W., Tufegdzic-Vidakovic, A. et al. (2016). A Biobank of breast cancer explants with preserved intra-tumor heterogeneity to screen anticancer compounds. *Cell* **167**, 260-274.e22. doi:10.1016/j.cell.2016.08.041

Brunker, J. and Beard, P. (2016). Velocity measurements in whole blood using acoustic resolution photoacoustic Doppler. *Biomed. Opt. Express* **7**, 2789-2806. doi:10.1364/BOE.7.002789

Brunker, J., Yao, J., Laufer, J. and Bohndiek, S. E. (2017). Photoacoustic imaging using genetically encoded reporters: a review. *J. Biomed. Opt.* **22**, 70901. doi:10.1117/1.JBO.22.7.070901

Calcinotto, A., Filipazzi, P., Grioni, M., Iero, M., De Milito, A., Ricupito, A., Cova, A., Canese, R., Jachetti, E., Rossetti, M. et al. (2012). Modulation of microenvironment acidity reverses anergy in human and murine tumor-infiltrating T lymphocytes. *Cancer Res.* **72**, 2746-2756. doi:10.1158/0008-5472.CAN-11-1272

Cao, Y., Kole, A., Hui, J., Zhang, Y., Mai, J., Alloosh, M., Sturek, M. and Cheng, J.-X. (2018). Fast assessment of lipid content in arteries in vivo by intravascular photoacoustic tomography. *Sci. Rep.* **8**, 2400. doi:10.1038/s41598-018-20881-5

Cerussi, A., Shah, N., Hsiang, D., Durkin, A., Butler, J. and Tromberg, B. J. (2006). In vivo absorption, scattering, and physiologic properties of 58 malignant breast tumors determined by broadband diffuse optical spectroscopy. *J. Biomed. Opt.* **11**, 044005. doi:10.1117/1.2337546

Chang, H. Y., Nuyten, D. S. A., Sneddon, J. B., Hastie, T., Tibshirani, R., Sørlie, T., Dai, H., He, Y. D., van't Veer, L. J., Bartelink, H. et al. (2005). Robustness, scalability, and integration of a wound-response gene expression signature in predicting breast cancer survival. *Proc. Natl. Acad. Sci. USA* **102**, 3738-3743. doi:10.1073/pnas.0409462102

Chatni, M. R., Yao, J., Danielli, A., Favazza, C. P., Maslov, K. I. and Wang, L. V. (2011). Functional photoacoustic microscopy of pH. *J. Biomed. Opt.* **16**, 100503. doi:10.1117/1.3644495

Chekkoury, A., Nunes, A., Gateau, J., Symvoulidis, P., Feuchtinger, A., Beziere, N., Ovsepian, S. V., Walch, A. and Ntziachristos, V. (2016). High-resolution multispectral optoacoustic tomography of the vascularization and constitutive hypoxemia of cancerous tumors. *Neoplasia* **18**, 459-467. doi:10.1016/j.neo.2016.06.004

Chen, Q., Liu, X., Chen, J., Zeng, J., Cheng, Z. and Liu, Z. (2015). A self-assembled albumin-based nanoprobe for in vivo ratiometric photoacoustic pH imaging. *Adv. Material* 27, 6820-6827. doi:10.1002/adma.201503194

Choi, S. Y. C., Lin, D., Gout, P. W., Collins, C. C., Xu, Y. and Wang, Y. (2014). Lessons from patient-derived xenografts for better in vitro modeling of human cancer. *Adv. Drug Deliv. Rev.* **79-80**, 222-237. doi:10.1016/j.addr.2014.09.009

Choi, J., Cha, Y. J. and Koo, J. S. (2018). Adipocyte biology in breast cancer: from silent bystander to active facilitator. *Prog. Lipid Res.* **69**, 11-20. doi:10.1016/j.plipres.2017.11.002

Colegio, O. R., Chu, N.-Q., Szabo, A. L., Chu, T., Rhebergen, A. M., Jairam, V., Cyrus, N., Brokowski, C. E., Eisenbarth, S. C., Phillips, G. M. et al. (2014). Functional polarization of tumour-associated macrophages by tumour-derived lactic acid. *Nature* **513**, 559. doi:10.1038/nature13490

Conklin, M. W., Eickhoff, J. C., Riching, K. M., Pehlke, C. A., Eliceiri, K. W., Provenzano, P. P., Friedl, A. and Keely, P. J. (2011). Aligned Collagen is a prognostic signature for survival in human breast carcinoma. *Am. J. Pathol.* **178**, 1221-1232. doi:10.1016/j.ajpath.2010.11.076

Costa, M., Shah, A., Rivens, I., Box, C., O'Shea, T., Bamber, J. and Ter Haar, G. (2018). Photoacoustic imaging for the prediction and assessment of response to radiotherapy in vivo. *bioRxiv* doi:10.1101/329516

Cox, B., Laufer, J. G., Arridge, S. R. and Beard, P. C. (2012). Quantitative spectroscopic photoacoustic imaging: a review. *J. Biomed. Opt.* **17**, 061202. doi:10.1117/1.JBO.17.6.061202
De Palma, M., Venneri, M. A., Roca, C. and Naldini, L. (2003). Targeting exogenous genes to tumor angiogenesis by transplantation of genetically modified hematopoietic stem cells. *Nat. Med.* **9**, 789. doi:10.1038/nm871
De Palma, M., Venneri, M. A., Galli, R., Sergi, L. S., Politi, L. S., Sampaolesi, M. and Naldini, L. (2005). Tie2 identifies a hematopoietic lineage of proangiogenic monocytes required for tumor vessel formation and a mesenchymal population of pericyte progenitors. *Cancer Cell* **8**, 211-226. doi:10.1016/j.ccr.2005.08.002
De Palma, M., Biziato, D. and Petrova, T. V. (2017). Microenvironmental regulation of tumour angiogenesis. *Nat. Rev. Cancer* **17**, 457. doi:10.1038/nrc.2017.51
Di Leo, G., Trimboli, R. M., Sella, T. and Sardanelli, F. (2017). Optical imaging of the breast: basic principles and clinical applications. *Am. J. Roentgenol.* **209**, 230-238. doi:10.2214/AJR.16.17220
Dickson, P. V., Hamner, J. B., Sims, T. L., Fraga, C. H., Ng, C. Y. C., Rajasekeran, S., Hagedorn, N. L., McCarville, M. B., Stewart, C. F. and Davidoff, A. M. (2007). Bevacizumab-induced transient remodeling of the vasculature in neuroblastoma xenografts results in improved delivery and efficacy of systemically administered chemotherapy. *Clin. Cancer Res.* **13**, 3942-3950. doi:10.1158/1078-0432.CCR-07-0278
Diot, G., Metz, S., Noske, A., Liapis, E., Schroeder, B., Ovsepian, S. V., Meier, R., Rummeny, E. J. and Ntziachristos, V. (2017). Multi-Spectral Optoacoustic Tomography (MSOT) of human breast cancer. *Clin. Cancer Res.* **23**, 6912-6922. doi:10.1158/1078-0432.CCR-16-3200
Dragulescu-Andrasi, A., Kothapalli, S.-R., Tikhomirov, G. A., Rao, J. and Gambhir, S. S. (2013). Activatable oligomerizable imaging agents for photoacoustic imaging of furin-like activity in living subjects. *J. Am. Chem. Soc.* **135**, 11015-11022. doi:10.1021/ja4010078
Egeblad, M. and Werb, Z. (2002). New functions for the matrix metalloproteinases in cancer progression. *Nat. Rev. Cancer* **2**, 161. doi:10.1038/nrc745
Erler, J. T., Bennewith, K. L., Nicolau, M., Dornhöfer, N., Kong, C., Le, Q.-T., Chi, J.-T. A., Jeffrey, S. S. and Giaccia, A. J. (2006). Lysyl oxidase is essential for hypoxia-induced metastasis. *Nature* **440**, 1222-1226. doi:10.1038/nature04695
Estrella, V., Chen, T., Lloyd, M., Wojtkowiak, J., Cornnell, H. H., Ibrahim-Hashim, A., Bailey, K., Balagurunathan, Y., Rothberg, J. M., Sloane, B. F. et al. (2013). Acidity generated by the tumor microenvironment drives local invasion. *Cancer Res.* **73**, 1524-1535. doi:10.1158/0008-5472.CAN-12-2796
Filippi, M., Garello, F., Pasquino, C., Arena, F., Giustetto, P., Antico, F. and Terreno, E. (2018). Indocyanine green labeling for optical and photoacoustic imaging of mesenchymal stem cells after in vivo transplantation. *J. Biophotonics* **12**, e201800035. doi:10.1002/jbio.201800035
Fleischer, A. C. (2000). Sonographic depiction of tumor vascularity and flow: from in vivo models to clinical applications. *J. Ultrasound Med.* **19**, 55-61. doi:10.7863/jum.2000.19.1.55
Folkman, J. (1971). Tumor angiogenesis: therapeutic implications. *N. Engl. J. Med.* **285**, 1182-1186. doi:10.1056/NEJM197111182852108
Franklin, R. A., Liao, W., Sarkar, A., Kim, M. V., Bivona, M. R., Liu, K., Pamer, E. G. and Li, M. O. (2014). The cellular and molecular origin of tumor-associated macrophages. *Science* **344**, 921-925. doi:10.1126/science.1252510
Fridman, W. H., Zitvogel, L., Sautès-Fridman, C. and Kroemer, G. (2017). The immune contexture in cancer prognosis and treatment. *Nat. Rev. Clin. Oncol.* **14**, 717. doi:10.1038/nrclinonc.2017.101
Gee, M. S., Saunders, H. M., Lee, J. C., Sanzo, J. F., Jenkins, W. T., Evans, S. M., Trinchieri, G., Sehgal, C. M., Feldman, M. D. and Lee, W. M. (2001). Doppler ultrasound imaging detects changes in tumor perfusion during antivascular therapy associated with vascular anatomic alterations. *Cancer Res.* **61**, 2974-2982.
Gerling, M., Zhao, Y., Nania, S., Norberg, K. J., Verbeke, C. S., Englert, B., Kuiper, R. V., Bergström, A., Hassan, M., Neesse, A. et al. (2014). Real-time assessment of tissue hypoxia In Vivo with combined photoacoustics and high-frequency ultrasound. *Theranostics* **4**, 604-613. doi:10.7150/thno.7996
Gibney, G. T., Weiner, L. M. and Atkins, M. B. (2016). Predictive biomarkers for checkpoint inhibitor-based immunotherapy. *Lancet. Oncol.* **17**, e542-e551. doi:10.1016/S1470-2045(16)30406-5
Gibson, H. M., McKnight, B. N., Malysa, A., Dyson, G., Wiesend, W. N., McCarthy, C. E., Reyes, J., Wei, W.-Z. and Viola-Villegas, N. T. (2018). IFNγ PET imaging as a predictive tool for monitoring response to tumor immunotherapy. *Cancer Res.* **78**, 5706-5717. doi:10.1158/0008-5472.CAN-18-0253
Giesel, F. L., Kratochwil, C., Lindner, T., Marschalek, M. M., Loktev, A., Lehnert, W., Debus, J., Jäger, D., Flechsig, P., Altmann, A. et al. (2019). 68Ga-FAPI PET/CT: biodistribution and preliminary dosimetry estimate of 2 DOTA-containing FAP-targeting agents in patients with various cancers. *J. Nucl. Med.* **60**, 386-392. doi:10.2967/jnumed.118.215913
Gilkes, D. M., Bajpai, S., Wong, C. C., Chaturvedi, P., Hubbi, M. E., Wirtz, D. and Semenza, G. L. (2013a). Procollagen lysyl hydroxylase 2 is essential for hypoxia-induced breast cancer metastasis. *Mol. Cancer Res.* **11**, 456-466. doi:10.1158/1541-7786.MCR-12-0629
Gilkes, D. M., Bajpai, S., Chaturvedi, P., Wirtz, D. and Semenza, G. L. (2013b). Hypoxia-inducible Factor 1 (HIF-1) promotes extracellular matrix remodeling under hypoxic conditions by inducing P4HA1, P4HA2, and PLOD2 expression in fibroblasts. *J. Biol. Chem.* **288**, 10819-10829. doi:10.1074/jbc.M112.442939
Gilkes, D. M., Semenza, G. L. and Wirtz, D. (2014). Hypoxia and the extracellular matrix: drivers of tumour metastasis. *Nat. Rev. Cancer* **14**, 430. doi:10.1038/nrc3726
Hallac, R. R., Zhou, H., Pidikiti, R., Song, K., Stojadinovic, S., Zhao, D., Solberg, T., Peschke, P. and Mason, R. P. (2014). Correlations of noninvasive BOLD and TOLD MRI with pO2 and relevance to tumor radiation response. *Magn. Reson. Med.* **71**, 1863-1873. doi:10.1002/mrm.24846
Hammoud, D. A. (2016). Molecular imaging of inflammation: current status. *J. Nucl. Med.* **57**, 1161-1165. doi:10.2967/jnumed.115.161182
Hanahan, D. and Weinberg, R. A. (2011). Hallmarks of cancer: the next generation. *Cell* **144**, 646-674. doi:10.1016/j.cell.2011.02.013
Hanna, R. N., Cekic, C., Sag, D., Tacke, R., Thomas, G. D., Nowyhed, H., Herrley, E., Rasquinha, N., McArdle, S., Wu, R. et al. (2015). Patrolling monocytes control tumor metastasis to the lung. *Science* **350**, 985-990. doi:10.1126/science.aac9407
Hanna, R. N., Chodaczek, G. and Hedrick, C. C. (2016). In vivo imaging of tumor and immune cell interactions in the lung. *Bio-protocol* **6**, e1973. doi:10.21769/BioProtoc.1973
Hasebe, T., Tsuda, H., Tsubono, Y., Imoto, S. and Mukai, K. (1997). Fibrotic focus in invasive ductal carcinoma of the breast: a histopathological prognostic parameter for tumor recurrence and tumor death within three years after the initial operation. *Jpn. J. Cancer Res.* **88**, 590-599. doi:10.1111/j.1349-7006.1997.tb00423.x
Hegde, P. S., Jubb, A. M., Chen, D., Li, N. F., Meng, Y. G., Bernaards, C., Elliott, R., Scherer, S. J. and Chen, D. S. (2013). Predictive impact of circulating vascular endothelial growth factor in four phase III trials evaluating Bevacizumab. *Clin. Cancer Res.* **19**, 929-937. doi:10.1158/1078-0432.CCR-12-2535
Heijblom, M., Piras, D., Brinkhuis, M., van Hespen, J. C. G., van den Engh, F. M., van der Schaaf, M., Klaase, J. M., van Leeuwen, T. G., Steenbergen, W. and Manohar, S. (2015). Photoacoustic image patterns of breast carcinoma and comparisons with Magnetic Resonance Imaging and vascular stained histopathology. *Sci. Rep.* **5**, 11778. doi:10.1038/srep11778
Heijblom, M., Piras, D., van den Engh, F. M., van der Schaaf, M., Klaase, J. M., Steenbergen, W. and Manohar, S. (2016). The state of the art in breast imaging using the Twente Photoacoustic Mammoscope: results from 31 measurements on malignancies. *Eur. Radiol.* **26**, 3874-3887. doi:10.1007/s00330-016-4240-7
Heiken, J. P. (2008). Contrast safety in the cancer patient: preventing contrast-induced nephropathy. *Cancer Imaging* **8**, S124-S127. doi:10.1102/1470-7330.2008.9018
Heldin, C.-H., Rubin, K., Pietras, K. and Östman, A. (2004). High interstitial fluid pressure — an obstacle in cancer therapy. *Nat. Rev. Cancer* **4**, 806. doi:10.1038/nrc1456
Hindelang, B., Aguirre, J., Schwarz, M., Berezhnoi, A., Eyerich, K., Ntziachristos, V., Biedermann, T. and Darsow, U. (2019). Non-invasive imaging in dermatology and the unique potential of raster-scan optoacoustic mesoscopy. *J. Eur. Acad. Dermatology Venereol.* **33**, 1051-1061. doi:10.1111/jdv.15342
Hobson-Gutierrez, S. A. and Carmona-Fontaine, C. (2018). The metabolic axis of macrophage and immune cell polarization. *Dis. Model. Mech.* **11**, dmm034462. doi:10.1242/dmm.034462
Hodi, F. S., O'Day, S. J., McDermott, D. F., Weber, R. W., Sosman, J. A., Haanen, J. B., Gonzalez, R., Robert, C., Schadendorf, D., Hassel, J. C. et al. (2010). Improved survival with ipilimumab in patients with metastatic melanoma. *N. Engl. J. Med.* **363**, 711-723. doi:10.1056/NEJMoa1003466
Hoeben, A., Landuyt, B., Highley, M. S., Wildiers, H., Van Oosterom, A. T. and De Bruijn, E. A. (2004). Vascular endothelial growth factor and angiogenesis. *Pharmacol. Rev.* **56**, 549-580. doi:10.1124/pr.56.4.3
Hoskin, P. J., Carnell, D. M., Taylor, N. J., Smith, R. E., Stirling, J. J., Daley, F. M., Saunders, M. I., Bentzen, S. M., Collins, D. J., D'Arcy, J. A. et al. (2007). Hypoxia in prostate cancer: correlation of BOLD-MRI with pimonidazole immunohistochemistry-initial observations. *Int. J. Radiat. Oncol. Biol. Phys.* **68**, 1065-1071. doi:10.1016/j.ijrobp.2007.01.018
Howe, F. A., Robinson, S. P., McIntyre, D. J. O., Stubbs, M. and Griffiths, J. R. (2001). Issues in flow and oxygenation dependent contrast (FLOOD) imaging of tumours. *NMR Biomed.* **14**, 497-506. doi:10.1002/nbm.716
Hughes, R., Qian, B.-Z., Rowan, C., Muthana, M., Keklikoglou, I., Olson, O. C., Tazzyman, S., Danson, S., Addison, C., Clemons, M. et al. (2015). Perivascular M2 macrophages stimulate tumor relapse after chemotherapy. *Cancer Res.* **75**, 3479-3491. doi:10.1158/0008-5472.CAN-14-3587
Imai, T., Muz, B., Yeh, C.-H., Yao, J., Zhang, R., Azab, A. K. and Wang, L. (2017). Direct measurement of hypoxia in a xenograft multiple myeloma model by optical-resolution photoacoustic microscopy. *Cancer Biol. Ther.* **18**, 101-105. doi:10.1080/15384047.2016.1276137
Jain, R. K., Martin, J. D. and Stylianopoulos, T. (2014). The role of mechanical forces in tumor growth and therapy. *Annu. Rev. Biomed. Eng.* **16**, 321-346. doi:10.1146/annurev-bioeng-071813-105259
Jansen, K., van der Steen, A. F. W., Wu, M., van Beusekom, H. M. M., Springeling, G., Li, X., Zhou, Q., Kirk Shung, K., de Kleijn, D. P. V. and van

Soest, G. (2014). Spectroscopic intravascular photoacoustic imaging of lipids in atherosclerosis. *J. Biomed. Opt.* **19**, 026006. doi:10.1117/1.JBO.19.2.026006
Jathoul, A. P., Laufer, J., Ogunlade, O., Treeby, B., Cox, B., Zhang, E., Johnson, P., Pizzey, A. R., Philip, B., Marafioti, T. et al. (2015). Deep in vivo photoacoustic imaging of mammalian tissues using a tyrosinase-based genetic reporter. *Nat. Photonics* **9**, 239-246. doi:10.1038/nphoton.2015.22
Jo, J., Lee, C. H., Kopelman, R. and Wang, X. (2017). In vivo quantitative imaging of tumor pH by nanosonophore assisted multispectral photoacoustic imaging. *Nat. Commun.* **8**, 471. doi:10.1038/s41467-017-00598-1
Joseph, J., Tomaszewski, M. R., Quiros-Gonzalez, I., Weber, J., Brunker, J. and Bohndiek, S. E. (2017). Evaluation of precision in optoacoustic tomography for preclinical imaging in living subjects. *J. Nucl. Med.* **58**, 807-814. doi:10.2967/jnumed.116.182311
Joyce, J. A. and Fearon, D. T. (2015). T cell exclusion, immune privilege, and the tumor microenvironment. *Science* **348**, 74-80. doi:10.1126/science.aaa6204
Kalluri, R. (2016). The biology and function of fibroblasts in cancer. *Nat. Rev. Cancer* **16**, 582. doi:10.1038/nrc.2016.73
Knieling, F., Neufert, C., Hartmann, A., Claussen, J., Urich, A., Egger, C., Vetter, M., Fischer, S., Pfeifer, L., Hagel, A. et al. (2017). Multispectral optoacoustic tomography for assessment of Crohn's disease activity. *N. Engl. J. Med.* **376**, 1292-1294. doi:10.1056/NEJMc1612455
Knox, H. J., Hedhli, J., Kim, T. W., Khalili, K., Dobrucki, L. W. and Chan, J. (2017). A bioreducible N-oxide-based probe for photoacoustic imaging of hypoxia. *Nat. Commun.* **8**, 1794. doi:10.1038/s41467-017-01951-0
Koch, C. J. and Evans, S. M. (2015). Optimizing hypoxia detection and treatment strategies. *Semin. Nucl. Med.* **45**, 163-176. doi:10.1053/j.semnuclmed.2014.10.004
Kostakoglu, L., Agress, H. and Goldsmith, S. J. (2003). Clinical role of FDG PET in evaluation of cancer patients. *Radiographics* **23**, 315-340. doi:10.1148/rg.232025705
Koyasu, S., Tsuji, Y., Harada, H., Nakamoto, Y., Nobashi, T., Kimura, H., Sano, K., Koizumi, K., Hamaji, M. and Togashi, K. (2016). Evaluation of tumor-associated stroma and its relationship with tumor hypoxia using dynamic contrast-enhanced CT and 18F Misonidazole PET in murine tumor models. *Radiology* **278**, 734-741. doi:10.1148/radiol.2015150416
Krishna Priya, S., Nagare, R. P., Sneha, V. S., Sidhanth, C., Bindhya, S., Manasa, P. and and Ganesan, T. S. (2016). Tumour angiogenesis—Origin of blood vessels. *Int. J. Cancer* **139**, 729-735. doi:10.1002/ijc.30067
Kruger, R. A., Kuzmiak, C. M., Lam, R. B., Reinecke, D. R., Del Rio, S. P. and Steed, D. (2016). Dedicated 3D photoacoustic breast imaging. *Med. Phys.* **40**, 113301. doi:10.1118/1.4824317
Krysan, K., Reckamp, K. L., Dalwadi, H., Sharma, S., Rozengurt, E., Dohadwala, M. and Dubinett, S. M. (2005). Prostaglandin E2 activates mitogen-activated protein kinase/Erk pathway signaling and cell proliferation in non-small cell lung cancer cells in an epidermal growth factor receptor-independent manner. *Cancer Res.* **65**, 6275-6281. doi:10.1158/0008-5472.CAN-05-0216
Kuhajda, F. P., Jenner, K., Wood, F. D., Hennigar, R. A., Jacobs, L. B., Dick, J. D. and Pasternack, G. R. (1994). Fatty acid synthesis: a potential selective target for antineoplastic therapy. *Proc. Natl. Acad. Sci.* **91**, 6379-6383. doi:10.1073/pnas.91.14.6379
LaGory, E. L. and Giaccia, A. J. (2016). The ever-expanding role of HIF in tumour and stromal biology. *Nat. Cell Biol.* **18**, 356. doi:10.1038/ncb3330
Lao, Y., Xing, D., Yang, S. and Xiang, L. (2008). Noninvasive photoacoustic imaging of the developing vasculature during early tumor growth. *Phys. Med. Biol.* **53**, 4203. doi:10.1088/0031-9155/53/15/013
Larimer, B. M., Wehrenberg-Klee, E., Caraballo, A. and Mahmood, U. (2016). Quantitative CD3 PET imaging predicts tumor growth response to anti-CTLA-4 therapy. *J. Nucl. Med.* **57**, 1607-1611. doi:10.2967/jnumed.116.173930
Larimer, B. M., Wehrenberg-Klee, E., Dubois, F., Mehta, A., Kalomeris, T., Flaherty, K., Boland, G. and Mahmood, U. (2017). Granzyme B PET imaging as a predictive biomarker of immunotherapy response. *Cancer Res.* **77**, 2318-2327. doi:10.1158/0008-5472.CAN-16-3346
Laufer, J., Johnson, P., Zhang, E., Treeby, B., Cox, B., Pedley, B. and Beard, P. (2012). In vivo preclinical photoacoustic imaging of tumor vasculature development and therapy. *J. Biomed. Opt.* **17**, 056016. doi:10.1117/1.JBO.17.5.056016
Lavaud, J., Henry, M., Coll, J. L. and Josserand, V. (2017). Exploration of melanoma metastases in mice brains using endogenous contrast photoacoustic imaging. *Int. J. Pharm.* **532**, 704-709. doi:10.1016/j.ijpharm.2017.08.104
LeBleu, V. S. and Kalluri, R. (2018). A peek into cancer-associated fibroblasts: origins, functions and translational impact. *Dis. Model. Mech.* **11**, dmm029447. doi:10.1242/dmm.029447
Lei, H., Johnson, L. A., Liu, S., Moons, D. S., Ma, T., Zhou, Q., Rice, M. D., Ni, J., Wang, X., Higgins, P. D. R. et al. (2016). Characterizing intestinal inflammation and fibrosis in Crohn's disease by photoacoustic imaging: feasibility study. *Biomed. Opt. Express* **7**, 2837-2848. doi:10.1364/BOE.7.002837
Levental, K. R., Yu, H., Kass, L., Lakins, J. N., Egeblad, M., Erler, J. T., Fong, S. F. T., Csiszar, K., Giaccia, A., Weninger, W. et al. (2009). Matrix crosslinking forces tumor progression by enhancing integrin signaling. *Cell* **139**, 891-906. doi:10.1016/j.cell.2009.10.027
Levi, J., Kothapalli, S.-R., Bohndiek, S., Yoon, J.-K., Dragulescu-Andrasi, A., Nielsen, C., Tisma, A., Bodapati, S., Gowrishankar, G., Yan, X. et al. (2013). Molecular photoacoustic imaging of follicular thyroid carcinoma. *Clin. Cancer Res.* **19**, 1494-1502. doi:10.1158/1078-0432.CCR-12-3061
Lewis, D. Y., Boren, J., Shaw, G. L., Bielik, R., Ramos-Montoya, A., Larkin, T. J., Martins, C. P., Neal, D. E., Soloviev, D. and Brindle, K. M. (2014). Late imaging with [1-11C]acetate improves detection of tumor fatty acid synthesis with PET. *J. Nucl. Med.* **55**, 1144-1149. doi:10.2967/jnumed.113.134437
Li, M.-N., Oh, J.-T., Xie, X., Ku, G., Wang, W., Li, C., Lungu, G., Stoica, G. and Wang, L. (2008). Simultaneous molecular and hypoxia imaging of brain tumors in vivo using spectroscopic photoacoustic tomography. *Proc. IEEE* **96**, 481-489. doi:10.1109/JPROC.2007.913515
Li, Y., Lin, R., Liu, C., Chen, J., Liu, H., Zheng, R., Gong, X. and Song, L. (2018). In vivo photoacoustic/ultrasonic dual-modality endoscopy with a miniaturized full field-of-view catheter. *J. Biophotonics* **11**, e201800034. doi:10.1002/jbio.201800034
Lin, L., Hu, P., Shi, J., Appleton, C. M., Maslov, K., Li, L., Zhang, R. and Wang, L. V. (2018). Single-breath-hold photoacoustic computed tomography of the breast. *Nat. Commun.* **9**, 2352. doi:10.1038/s41467-018-04576-z
Lopci, E., Grassi, I., Chiti, A., Nanni, C., Cicoria, G., Toschi, L., Fonti, C., Lodi, F., Mattioli, S. and Fanti, S. (2014). PET radiopharmaceuticals for imaging of tumor hypoxia: a review of the evidence. *Am. J. Nucl. Med. Mol. Imaging* **4**, 365-384.
Lu, P., Weaver, V. M. and Werb, Z. (2012). The extracellular matrix: a dynamic niche in cancer progression. *J. Cell Biol.* **196**, 395-406. doi:10.1083/jcb.201102147
Lundgren, K., Holm, C. and Landberg, G. (2007). Common molecular mechanisms of mammary gland development and breast cancer. *Cell. Mol. Life Sci.* **64**, 3233-3247. doi:10.1007/s00018-007-7390-6
Manohar, S., Kharine, A., van Hespen, J. C. G., Steenbergen, W. and van Leeuwen, T. G. (2005). The Twente Photoacoustic Mammoscope: system overview and performance. *Phys. Med. Biol.* **50**, 2543. doi:10.1088/0031-9155/50/11/007
Martinho Costa, M., Shah, A., Rivens, I., Box, C., O'Shea, T., Papaevangelou, E., Bamber, J. and Ter Haar, G. (2018). Quantitative photoacoustic imaging study of tumours in vivo: baseline variations in quantitative measurements. *Photoacoustics* **13**, 53-65. doi:10.1016/j.pacs.2018.12.002
Maute, R. L., Gordon, S. R., Mayer, A. T., McCracken, M. N., Natarajan, A., Ring, N. G., Kimura, R., Tsai, J. M., Manglik, A., Kruse, A. C. et al. (2015). Engineering high-affinity PD-1 variants for optimized immunotherapy and immuno-PET imaging. *Proc. Natl. Acad. Sci. USA* **112**, E6506-E6514. doi:10.1073/pnas.1519623112
Mehnert, J. M., Monjazeb, A. M., Beerthuijzen, J. M. T., Collyar, D., Rubinstein, L. and Harris, L. N. (2017). The challenge for development of valuable immuno-oncology biomarkers. *Clin. Cancer Res.* **23**, 4970-4979. doi:10.1158/1078-0432.CCR-16-3063
Meir, R., Motiei, M. and Popovtzer, R. (2014). Gold nanoparticles for in vivo cell tracking. *Nanomedicine* **9**, 2059-2069. doi:10.2217/nnm.14.129
Menezes, G. L. G., Pijnappel, R. M., Meeuwis, C., Bisschops, R., Veltman, J., Lavin, P. T., van de Vijver, M. J. and Mann, R. M. (2018). Downgrading of breast masses suspicious for cancer by using optoacoustic breast imaging. *Radiology* **288**, 355-365. doi:10.1148/radiol.2018170500
Michiels, C., Tellier, C. and Feron, O. (2016). Cycling hypoxia: a key feature of the tumor microenvironment. *Biochim. Biophys. Acta Rev. Cancer* **1866**, 76-86. doi:10.1016/j.bbcan.2016.06.004
Morton, J. J., Bird, G., Refaeli, Y. and Jimeno, A. (2016). Humanized mouse xenograft models: narrowing the tumor-microenvironment gap. *Cancer Res.* **76**, 6153-6158. doi:10.1158/0008-5472.CAN-16-1260
Muzard, J., Sarda-Mantel, L., Loyau, S., Meulemans, A., Louedec, L., Bantsimba-Malanda, C., Hervatin, F., Marchal-Somme, J., Michel, J. B., Le Guludec, D. et al. (2009). Non-invasive molecular imaging of fibrosis using a collagen-targeted peptidomimetic of the platelet collagen receptor glycoprotein VI. *PLoS ONE* **4**, e5585-e5585. doi:10.1371/journal.pone.0005585
Nagy, J. A. and Dvorak, H. F. (2012). Heterogeneity of the tumor vasculature: the need for new tumor blood vessel type-specific targets. *Clin. Exp. Metastasis* **29**, 657-662. doi:10.1007/s10585-012-9500-6
Nagy, J. A., Dvorak, A. M. and Dvorak, H. F. (2007). VEGF-A and the induction of pathological angiogenesis. *Annu. Rev. Pathol. Mech. Dis.* **2**, 251-275. doi:10.1146/annurev.pathol.2.010506.134925
Nakajima, M., Nagahashi, M., Rashid, O. M., Takabe, K. and Wakai, T. (2017). The role of sphingosine-1-phosphate in the tumor microenvironment and its clinical implications. *Tumor Biol.* **39**, 1010428317699133. doi:10.1177/1010428317699133
Natarajan, A., Mayer, A. T., Reeves, R. E., Nagamine, C. M. and Gambhir, S. S. (2017). Development of novel immunoPET tracers to image human PD-1 checkpoint expression on tumor-infiltrating lymphocytes in a humanized mouse model. *Mol. Imaging Biol.* **19**, 903-914. doi:10.1007/s11307-017-1060-3
Neuschler, E. I., Butler, R., Young, C. A., Barke, L. D., Bertrand, M. L., Böhm-Vélez, M., Destounis, S., Donlan, P., Grobmyer, S. R., Katzen, J. et al. (2018). A pivotal study of optoacoustic imaging to diagnose benign and malignant breast masses: a new evaluation tool for radiologists. *Radiology* **287**, 398-412. doi:10.1148/radiol.2017172228

Neuschmelting, V., Burton, N. C., Lockau, H., Urich, A., Harmsen, S., Ntziachristos, V. and Kircher, M. F. (2016). Performance of a Multispectral Optoacoustic Tomography (MSOT) system equipped with 2D vs. 3D handheld probes for potential clinical translation. *Photoacoustics* **4**, 1-10. doi:10.1016/j.pacs.2015.12.001

Nishino, M., Hatabu, H. and Hodi, F. S. (2018). Imaging of cancer immunotherapy: current approaches and future directions. *Radiology* **290**, 9-22. doi:10.1148/radiol.2018181349

Ntziachristos, V., Ripoll, J., Wang, L. V. and Weissleder, R. (2005). Looking and listening to light: the evolution of whole-body photonic imaging. *Nat. Biotechnol.* **23**, 313. doi:10.1038/nbt1074

O'Connor, J. P. B., Boult, J. K. R., Jamin, Y., Babur, M., Finegan, K. G., Williams, K. J., Little, R. A., Jackson, A., Parker, G. J. M., Reynolds, A. R. et al. (2016). Oxygen-enhanced MRI accurately identifies, quantifies, and maps tumor hypoxia in preclinical cancer models. *Cancer Res.* **76**, 787-795. doi:10.1158/0008-5472.CAN-15-2062

O'Connor, J. P. B., Aboagye, E. O., Adams, J. E., Aerts, H. J. W. L., Barrington, S. F., Beer, A. J., Boellaard, R., Bohndiek, S. E., Brady, M., Brown, G. et al. (2017). Imaging biomarker roadmap for cancer studies. *Nat. Rev. Clin. Oncol.* **14**, 169-186. doi:10.1038/nrclinonc.2016.162

Ohno, Y., Nishio, M., Koyama, H., Miura, S., Yoshikawa, T., Matsumoto, S. and Sugimura, K. (2014). Dynamic contrast-enhanced CT and MRI for pulmonary nodule assessment. *Am. J. Roentgenol.* **202**, 515-529. doi:10.2214/AJR.13.11888

Omar, M., Schwarz, M., Soliman, D., Symvoulidis, P. and Ntziachristos, V. (2015). Pushing the optical imaging limits of cancer with multi-frequency-band raster-scan optoacoustic mesoscopy (RSOM). *Neoplasia* **17**, 208-214. doi:10.1016/j.neo.2014.12.010

Parks, S. K. and Pouysségur, J. (2017). Targeting pH regulating proteins for cancer therapy–Progress and limitations. *Semin. Cancer Biol.* **43**, 66-73. doi:10.1016/j.semcancer.2017.01.007

Parks, S. K., Chiche, J. and Pouyssegur, J. (2010). pH control mechanisms of tumor survival and growth. *J. Cell. Physiol.* **226**, 299-308. doi:10.1002/jcp.22400

Pokharel, S. S., Macura, K. J., Kamel, I. R. and Zaheer, A. (2013). Current MR imaging lipid detection techniques for diagnosis of lesions in the abdomen and pelvis. *Radiographics* **33**, 681-702. doi:10.1148/rg.333125068

Postema, A., Mischi, M., de la Rosette, J. and Wijkstra, H. (2015). Multiparametric ultrasound in the detection of prostate cancer: a systematic review. *World J. Urol.* **33**, 1651-1659. doi:10.1007/s00345-015-1523-6

Pyne, N. J. and Pyne, S. (2010). Sphingosine 1-phosphate and cancer. *Nat. Rev. Cancer* **10**, 489. doi:10.1038/nrc2875

Qu, Y., Li, C., Shi, J., Chen, R., Xu, S., Rafsanjani, H., Maslov, K., Krigman, H., Garvey, L., Hu, P. et al. (2018). Transvaginal fast-scanning optical-resolution photoacoustic endoscopy. *J. Biomed. Opt.* **23**, 1-4. doi:10.1117/1.JBO.23.12.121617

Quail, D. F. and Joyce, J. A. (2013). Microenvironmental regulation of tumor progression and metastasis. *Nat. Med.* **19**, 1423. doi:10.1038/nm.3394

Quiros-Gonzalez, I., Tomaszewski, M. R., Aitken, S. J., Ansel-Bollepalli, L., McDuffus, L.-A., Gill, M., Hacker, L., Brunker, J. and Bohndiek, S. E. (2018). Optoacoustics delineates murine breast cancer models displaying angiogenesis and vascular mimicry. *Br. J. Cancer* **118**, 1098-1106. doi:10.1038/s41416-018-0033-x

Qureshi, N. R., Shah, A., Eaton, R. J., Miles, K., Gilbert, F. J. and **on behalf of the Sputnik Investigators**. (2016). Dynamic contrast enhanced CT in nodule characterization: How we review and report. *Cancer Imaging* **16**, 16. doi:10.1186/s40644-016-0074-4

Raes, F., Sobilo, J., Le Mée, M., Rétif, S., Natkunarajah, S., Lerondel, S. and Le Pape, A. (2016). High resolution ultrasound and photoacoustic imaging of orthotopic lung cancer in mice: new perspectives for onco-pharmacology. *PLoS ONE* **11**, e0153532. doi:10.1371/journal.pone.0153532

Ramamonjisoa, N. and Ackerstaff, E. (2017). Characterization of the tumor microenvironment and tumor-stroma interaction by non-invasive preclinical imaging. *Front. Oncol.* **7**, 3. doi:10.3389/fonc.2017.00003

Ribeiro, A. L. and Okamoto, O. K. (2015). Combined effects of pericytes in the tumor microenvironment. *Stem Cells Int.* **2015**, 868475. doi:10.1155/2015/868475

Rich, L. J. and Seshadri, M. (2016). Photoacoustic monitoring of tumor and normal tissue response to radiation. *Sci. Rep.* **6**, 21237. doi:10.1038/srep21237

Rofstad, E. K., Mathiesen, B., Kindem, K. and Galappathi, K. (2006). Acidic extracellular pH promotes experimental metastasis of human melanoma cells in athymic nude mice. *Cancer Res.* **66**, 6699-6707. doi:10.1158/0008-5472.CAN-06-0983

Rogosnitzky, M. and Branch, S. (2016). Gadolinium-based contrast agent toxicity: a review of known and proposed mechanisms. *Biometals* **29**, 365-376. doi:10.1007/s10534-016-9931-7

Rosenberg, S. A. and Restifo, N. P. (2015). Adoptive cell transfer as personalized immunotherapy for human cancer. *Science* **348**, 62-68. doi:10.1126/science.aaa4967

Saini, R. and Hoyt, K. (2014). Recent developments in dynamic contrast-enhanced ultrasound imaging of tumor angiogenesis. *Imaging Med.* **6**, 41-52. doi:10.2217/iim.13.74

Saupe, F., Schwenzer, A., Jia, Y., Gasser, I., Spenlé, C., Langlois, B., Kammerer, M., Lefebvre, O., Hlushchuk, R., Rupp, T. et al. (2013). Tenascin-C downregulates Wnt inhibitor Dickkopf-1, promoting tumorigenesis in a neuroendocrine tumor model. *Cell Rep.* **5**, 482-492. doi:10.1016/j.celrep.2013.09.014

Schöder, H. and Larson, S. M. (2004). Positron emission tomography for prostate, bladder, and renal cancer. *Semin. Nucl. Med.* **34**, 274-292. doi:10.1053/j.semnuclmed.2004.06.004

Schuurhuis, D. H., Verdijk, P., Schreibelt, G., Aarntzen, E. H. J. G., Scharenborg, N., de Boer, A., van de Rakt, M. W. M. M., Kerkhoff, M., Gerritsen, M.-J. P., Eijckeler, F. et al. (2009). In situ expression of tumor antigens by messenger RNA electroporated dendritic cells in lymph nodes of melanoma patients. *Cancer Res.* **69**, 2927-2934. doi:10.1158/0008-5472.CAN-08-3920

Sehgal, C. M., Arger, P. H., Rowling, S. E., Conant, E. F., Reynolds, C. and Patton, J. A. (2000). Quantitative vascularity of breast masses by Doppler imaging: regional variations and diagnostic implications. *J. Ultrasound Med.* **19**, 427-440. doi:10.7863/jum.2000.19.7.427

Semenza, G. L. (2016). The hypoxic tumor microenvironment: a driving force for breast cancer progression. *Biochim. Biophys. Acta Mol. Cell Res.* **1863**, 382-391. doi:10.1016/j.bbamcr.2015.05.036

Sharma, P. and Allison, J. P. (2015). The future of immune checkpoint therapy. *Science* **348**, 56-61. doi:10.1126/science.aaa8172

Shultz, L. D., Ishikawa, F. and Greiner, D. L. (2007). Humanized mice in translational biomedical research. *Nat. Rev. Immunol.* **7**, 118. doi:10.1038/nri2017

Steinberg, I., Hulandad, D. M., Vermesh, O., Frostig, H. E., Tummers, W. S. and Gambhir, S. S. (2019). Photoacoustic clinical imaging. *Photoacoustics* **14**, 77-98. doi:10.1016/j.pacs.2019.05.001

Stockmann, C., Doedens, A., Weidemann, A., Zhang, N., Takeda, N., Greenberg, J. I., Cheresh, D. A. and Johnson, R. S. (2008). Deletion of vascular endothelial growth factor in myeloid cells accelerates tumorigenesis. *Nature* **456**, 814. doi:10.1038/nature07445

Talwalkar, J. A., Kurtz, D. M., Schoenleber, S. J., West, C. P. and Montori, V. M. (2007). Ultrasound-based transient elastography for the detection of hepatic fibrosis: systematic review and meta-analysis. *Clin. Gastroenterol. Hepatol.* **5**, 1214-1220. doi:10.1016/j.cgh.2007.07.020

Taouli, B., Tolia, A. J., Losada, M., Babb, J. S., Chan, E. S., Bannan, M. A. and Tobias, H. (2007). Diffusion-weighted MRI for quantification of liver fibrosis: preliminary experience. *Am. J. Roentgenol.* **189**, 799-806. doi:10.2214/AJR.07.2086

Tavaré, R., McCracken, M. N., Zettlitz, K. A., Knowles, S. M., Salazar, F. B., Olafsen, T., Witte, O. N. and Wu, A. M. (2014). Engineered antibody fragments for immuno-PET imaging of endogenous CD8+ T cells in vivo. *Proc. Natl. Acad. Sci. USA* **111**, 1108-1113. doi:10.1073/pnas.1316922111

Toi, M., Asao, Y., Matsumoto, Y., Sekiguchi, H., Yoshikawa, A., Takada, M., Kataoka, M., Endo, T., Kawaguchi-Sakita, N., Kawashima, M. et al. (2017). Visualization of tumor-related blood vessels in human breast by photoacoustic imaging system with a hemispherical detector array. *Sci. Rep.* **7**, 41970. doi:10.1038/srep41970

Tomaszewski, M. R., Gonzalez, I. Q., O'Connor, J. P. B., Abeyakoon, O., Parker, G. J. M., Williams, K. J., Gilbert, F. J. and Bohndiek, S. E. (2017). Oxygen Enhanced Optoacoustic Tomography (OE-OT) reveals vascular dynamics in murine models of prostate cancer. *Theranostics* **7**, 2900-2913. doi:10.7150/thno.19841

Tomaszewski, M. R., Gehrung, M., Joseph, J., Quiros-Gonzalez, I., Disselhorst, J. A. and Bohndiek, S. E. (2018). Oxygen-enhanced and dynamic contrast-enhanced optoacoustic tomography provide surrogate biomarkers of tumor vascular function, hypoxia, and necrosis. *Cancer Res.* **78**, 5980-5991. doi:10.1158/0008-5472.CAN-18-1033

Trédan, O., Galmarini, C. M., Patel, K. and Tannock, I. F. (2007). Drug resistance and the solid tumor microenvironment. *J. Natl. Cancer Inst.* **99**, 1441-1454. doi:10.1093/jnci/djm135

Tromberg, B. J., Cerussi, A., Shah, N., Compton, M., Durkin, A., Hsiang, D., Butler, J. and Mehta, R. (2005). Imaging in breast cancer: Diffuse optics in breast cancer: detecting tumors in pre-menopausal women and monitoring neoadjuvant chemotherapy. *Breast Cancer Res.* **7**, 279. doi:10.1186/bcr1358

Tzoumas, S., Zaremba, A., Klemm, U., Nunes, A., Schaefer, K. and Ntziachristos, V. (2014). Immune cell imaging using multi-spectral optoacoustic tomography. *Opt. Lett.* **39**, 3523-3526. doi:10.1364/OL.39.003523

van den Berg, P. J., Daoudi, K. and Steenbergen, W. (2015). Review of photoacoustic flow imaging: its current state and its promises. *Photoacoustics* **3**, 89-99. doi:10.1016/j.pacs.2015.08.001

van den Berg, P. J., Bansal, R., Daoudi, K., Steenbergen, W. and Prakash, J. (2016). Preclinical detection of liver fibrosis using dual-modality photoacoustic/ultrasound system. *Biomed. Opt. Express* **7**, 5081-5091. doi:10.1364/BOE.7.005081

van der Veldt, A. A. M., Hendrikse, N. H., Harms, H. J., Comans, E. F. I., Postmus, P. E., Smit, E. F., Lammertsma, A. A. and Lubberink, M. (2010).

Quantitative parametric perfusion images using 15O-labeled water and a clinical PET/CT scanner: test–retest variability in lung cancer. *J. Nucl. Med.* **51**, 1684-1690. doi:10.2967/jnumed.110.079137

Venkatesh, S. K., Yin, M., Glockner, J. F., Takahashi, N., Araoz, P. A., Talwalkar, J. A. and Ehman, R. L. (2008). MR elastography of liver tumors: preliminary results. *Am. J. Roentgenol.* **190**, 1534-1540. doi:10.2214/AJR.07.3123

Vukovic, V. and Tannock, I. F. (1997). Influence of low pH on cytotoxicity of paclitaxel, mitoxantrone and topotecan. *Br. J. Cancer* **75**, 1167-1172. doi:10.1038/bjc.1997.201

Walter, K., Hong, S.-M., Nyhan, S., Canto, M., Fedarko, N., Klein, A., Griffith, M., Omura, N., Medghalchi, S., Kuhajda, F. et al. (2009). Serum fatty acid synthase as a marker of pancreatic neoplasia. *Cancer Epidemiol. Prev. Biomarkers* **18**, 2380-2385. doi:10.1158/1055-9965.EPI-09-0144

Wang, L. V. and Hu, S. (2012). Photoacoustic tomography: in vivo imaging from organelles to organs. *Science* **335**, 1458-1462. doi:10.1126/science.1216210

Wang, L. V. and Yao, J. (2016). A practical guide to photoacoustic tomography in the life sciences. *Nat. Methods* **13**, 627-638. doi:10.1038/nmeth.3925

Wang, B., Karpiouk, A., Yeager, D., Amirian, J., Litovsky, S., Smalling, R. and Emelianov, S. (2012). In vivo intravascular ultrasound-guided photoacoustic imaging of lipid in plaques using an animal model of atherosclerosis. *Ultrasound Med. Biol.* **38**, 2098-2103. doi:10.1016/j.ultrasmedbio.2012.08.006

Waterhouse, D. J., Fitzpatrick, C. R. M., Pogue, B. W., O'Connor, J. P. B. and Bohndiek, S. E. (2019). A roadmap for the clinical implementation of optical-imaging biomarkers. *Nat Biomed. Eng.* **3**, 339-353. doi:10.1038/s41551-019-0392-5

Weber, J., Beard, P. C. and Bohndiek, S. E. (2016). Contrast agents for molecular photoacoustic imaging. *Nat. Methods* **13**, 639-650. doi:10.1038/nmeth.3929

Weissleder, R., Schwaiger, M. C., Gambhir, S. S. and Hricak, H. (2016). Imaging approaches to optimize molecular therapies. *Sci. Transl. Med.* **8**, 355ps16. doi:10.1126/scitranslmed.aaf3936

Wilson, K. E., Bachawal, S. V., Tian, L. and Willmann, J. K. (2014). Multiparametric spectroscopic photoacoustic imaging of breast cancer development in a transgenic mouse model. *Theranostics* **4**, 1062-1071. doi:10.7150/thno.9922

Winkler, F., Kozin, S. V., Tong, R. T., Chae, S.-S., Booth, M. F., Garkavtsev, I., Xu, L., Hicklin, D. J., Fukumura, D., di Tomaso, E. et al. (2004). Kinetics of vascular normalization by VEGFR2 blockade governs brain tumor response to radiation: Role of oxygenation, angiopoietin-1, and matrix metalloproteinases. *Cancer Cell* **6**, 553-563. doi:10.1016/s1535-6108(04)00305-8

Wu, C., Li, F., Niu, G. and Chen, X. (2013). PET imaging of inflammation biomarkers. *Theranostics* **3**, 448-466. doi:10.7150/thno.6592

Wu, M., Jansen, K., van der Steen, A. F. W. and van Soest, G. (2015). Specific imaging of atherosclerotic plaque lipids with two-wavelength intravascular photoacoustics. *Biomed. Opt. Express* **6**, 3276-3286. doi:10.1364/BOE.6.003276

Xu, Y., Zhu, L., Ru, T., Wang, H., He, J., Zhou, Z. and Yang, X. (2017). Three-dimensional power Doppler ultrasound in the early assessment of response to concurrent chemo-radiotherapy for advanced cervical cancer. *Acta Radiol.* **58**, 1147-1154. doi:10.1177/0284185116684677

Yamaga, I., Kawaguchi-Sakita, N., Asao, Y., Matsumoto, Y., Yoshikawa, A., Fukui, T., Takada, M., Kataoka, M., Kawashima, M., Fakhrejahani, E. et al. (2018). Vascular branching point counts using photoacoustic imaging in the superficial layer of the breast: a potential biomarker for breast cancer. *Photoacoustics* **11**, 6-13. doi:10.1016/j.pacs.2018.06.002

Yao, J., Kaberniuk, A. A., Li, L., Shcherbakova, D. M., Zhang, R., Wang, L., Li, G., Verkhusha, V. V. and Wang, L. V. (2015). Multiscale photoacoustic tomography using reversibly switchable bacterial phytochrome as a near-infrared photochromic probe. *Nat. Methods* **13**, 67-73. doi:10.1038/nmeth.3656

Yin, C., Wen, G., Liu, C., Yang, B., Lin, S., Huang, J., Zhao, P., Wong, S. H. D., Zhang, K., Chen, X. et al. (2018). Organic semiconducting polymer nanoparticles for photoacoustic labeling and tracking of stem cells in the second near-infrared window. *ACS Nano* **12**, 12201-12211. doi:10.1021/acsnano.8b05906

Yin, L., Sun, H., Zhang, H., He, L., Qiu, L., Lin, J., Xia, H., Zhang, Y., Ji, S., Shi, H. et al. (2019). Quantitatively visualizing tumor-related protease activity in vivo using a ratiometric photoacoustic probe. *J. Am. Chem. Soc.* **141**, 3265-3273. doi:10.1021/jacs.8b13628

Yoon, T.-J. and Cho, Y.-S. (2013). Recent advances in photoacoustic endoscopy. *World J. Gastrointest. Endosc.* **5**, 534-539. doi:10.4253/wjge.v5.i11.534

Zhan, Y., Ginanni, N., Tota, M. R., Wu, M., Bays, N. W., Richon, V. M., Kohl, N. E., Bachman, E. S., Strack, P. R. and Krauss, S. (2008). Control of cell growth and survival by enzymes of the fatty acid synthesis pathway in HCT-116 colon cancer cells. *Clin. Cancer Res.* **14**, 5735-5742. doi:10.1158/1078-0432.CCR-07-5074

Zhang, K., Corsa, C. A., Ponik, S. M., Prior, J. L., Piwnica-Worms, D., Eliceiri, K. W., Keely, P. J. and Longmore, G. D. (2013). The Collagen receptor discoidin domain receptor 2 stabilizes SNAIL1 to facilitate breast cancer metastasis. *Nat. Cell Biol.* **15**, 677-687. doi:10.1038/ncb2743

Zheng, S., Li, H., Lai, K., Chen, M., Fu, G., Liu, W.-H., Fu, G. and Nie, L. (2018). Noninvasive photoacoustic and fluorescent tracking of optical dye labeled T cellular activities of diseased sites at new depth. *J. Biophotonics* **11**, e201800073. doi:10.1002/jbio.201800073

Zhu, Y., Johnson, L. A., Huang, Z., Rubin, J. M., Yuan, J., Lei, H., Ni, J., Wang, X., Higgins, P. D. R. and Xu, G. (2018). Identifying intestinal fibrosis and inflammation by spectroscopic photoacoustic imaging: an animal study in vivo. *Biomed. Opt. Express* **9**, 1590-1600. doi:10.1364/BOE.9.001590